

**A study on the effect of the synthesis variables of mechano-chemically synthesized ZSM-5
on its physicochemical properties**

Julieth Tatiana García Sánchez

**Research work presented as a requirement to apply for the degree of
Ingeniera Química**

Advisor

**Víctor Baldovino Medrano
Chemical engineer, PhD.**

Co- advisor

**Iván Darío Mora Vergara
Chemical engineer, MSc.**

**Universidad Industrial de Santander
Facultad de Ingenierías Físicoquímicas
Escuela de ingeniería química
Bucaramanga**

2020

Dedicated to

To God, for giving wisdom and patience always.

*To my mom, for being my guide and support. For giving me the example that only
through effort do dreams come true.*

*To my siblings and my family for being the engine that drives me to move forward
despite the adversities.*

*To Isa, Lu, Andre, Lalis, Nico, Pacho, Nata, Angie, Cata and Cami, who are my
second family and showed me not only the value of friendship, but that, despite the differences,
adversities and the distance will always be there for me.*

*To Camila, for always being by my side regardless of the circumstances, for
motivating me every day to fulfill my dreams and teach me to believe in myself and everything
I can achieve.*

Acknowledgements

To Professor Víctor Baldovino and Magister Iván Mora for their collaboration, patience and constant teaching, which not only contributed to the development of this project, but also to my life.

To the CICAT's members of the for giving me their support, advice and experiences, which enriched my learning.

To the Industrial University of Santander and the School of Chemical Engineering for the countless experiences, which allowed me to train as a professional and as a person.

To the scanning electron microscopy (SEM) and X-ray diffraction (XRD) laboratories of the Industrial University of Santander for providing services for the development of this project.

Contents

Introduction.....	13
1. Objectives.....	18
1.1 General objective.....	18
1.2. Specific objectives.....	18
2. Experimental section.....	18
2.1 Materials synthesis.....	19
2.2. Assesment of physicochemical properties.....	21
2.3. Catalytic tests.....	23
2.3.1.Catalysts activation.....	23
2.3.2.Reaction procedure.....	23
3. Results and discussion.....	24
3.1. Materials properties.....	24
3.1.1. Morphology and chemical composition.....	25
3.1.2. Materials crystallinity.....	28
3.1.3. Porosity and surface area.....	32
3.1.4. Acidity of the materials.....	35
3.2. Catalytic performance.....	37
4. Conclusions.....	39

5. Recommendations	39
6. Participation in events	40
References	41
Appendix	48

List of figures

Figure 1. ZSM-5 zeolite, (a) zeolite structure, (b) pentasil units, (c) porous channels structure ...	14
Figure 2. Phenol alkylation with tert-butyl alcohol using as a catalyst a ZSM-5 zeolite, reaction scheme (Jiang, y otros, 2015) (Adam, Hello, & Ali, 2011) .tert-butyl phenyl ether (t-BPE), 2-tert-butyl-phenol (2-TBP), 4-tert-butyl-phenol (4-TBP), 3-tert-butyl-phenol (3-TBP), 2,4-di-tert-butyl phenol (2,4-DTBP) and 2,4,6-tri-tert-butyl phenol(2,4,6-TTBP)	17
Figure 3. Methodological stages of the project	19
Figure 4. Experimental set-up for the test of alkylation of phenol with tert-butyl alcohol.....	24
Figure 5. Micrographs of the seed (CBV 2314) with cubic shaped crystals and mordenite impurities with rod shapes.....	25
Figure 6. Effect of the crystallization on the morphological properties a) before crystallization (Z-t0) and b) after crystallization (Z-Na0.2-T5-S200-H1.7).....	26
Figure 7. Selected SEM images for samples of the materials synthesized under the following conditions a) Z-Na0.2-T20-S200-H2.0, b) Z-Na0.2-T20-S400-H2.0, c) Z-Na0.2-T5-S400-H1.7, d) Z-Na0.2-T20-S400-H1.7 e) Z-Na0.2-T20-S200-H1.7 and f) Z-Na0.2-T20-S200-H2.0	27
Figure 8. Molar composition and Si/Al ratio of samples synthesized under the following conditions: a) CBV 2314 b), c) Z-Na0.2-T5-S200-H2.0 d) Z-Na0.2-T5-S400- H1.7 and e) Z-Na0.2-T20-S400-H1.7	28
Figure 9. XRD patterns of synthesized zeolites a) ZSM-5 phase identification and b) mordenite phase impurity peaks	29
Figure 10. ATR-FTIR spectra with the presence of the characteristic bands of the ZSM-5 in the synthesized samples, the seed and the sample before the crystallization stage.	31

Figure 11. Main effects on the percentage of crystallinity of synthesized materials a) milling speed, b) H ₂ O/SiO ₂ ratio and c) milling time.	32
Figure 12. χ method Ar adsorption-desorption isotherms of the synthesized samples: a) Z-Na0.2-T5-S200-H1.7, b) Z-Na0.2-T5-S200-H2.0, c) Z-Na0.2-T5-S400-H1.7, d) Z-Na0.2-T5-S400-H2.0, e) Z-Na0.2-T20-S200-H1.7, f) Z-Na0.2-T20-S200-H2.0, g) Z-Na0.2-T20-S400-H1.7, h) Z-Na0.2-T5-S400-H2.0 and i) CBV 2314.	33
Figure 13. Main effects on the surface area of synthesized materials a) milling speed, b) H ₂ O/SiO ₂ and c) milling time.	34
Figure 14. FTIR spectra for pyridine TPD recorded of CBV 2314 at 298, 373, 473 and 623 K. The highlighted bands correspond to pyridine adsorption on Brønsted (1545 cm ⁻¹) and Lewis sites (1455 cm ⁻¹). Band at 1491 cm ⁻¹ corresponds to an overlap of the signals from pyridine adsorbed on both the Brønsted and the Lewis sites and the band found at 1445 cm ⁻¹ corresponds to the physically adsorbed pyridine (Buzzoni, Bordiga, Ricchiardi, Lamberti, & Zecchina, 1996).	36
Figure 15. Main effects on the total acid sites concentration of synthesized materials a) milling time, b) H ₂ O/SiO ₂ and c) milling speed.	36
Figure 16. Main effects on phenol conversion a) milling time, b) H ₂ O/SiO ₂ and c) milling speed.	38

List of tables

Table 1. Experimental design.....	20
Table 2. Order of execution of the experiments.....	21
Table 3. Crystallinity, ZSM-5 and mordenite percentage of the synthesized samples and the seed	32
Table 4. Synthesized materials properties	34
Table 5. Concentration of total acid sites and of the Brønsted and Lewis sites for the synthesized samples and the seed, according to pyridine TPD test. [mmol/g].....	37
Table 6. Conversion and selectivity of the phenol alkylation with tert-butyl alcohol for each synthesized zeolite and the seed.....	38

List of appendix

Appendix A. Ar (87 k) adsorption-desorption isotherms and pore size distribution of the synthesized samples.....	48
Appendix B. Anova tables and double and triple effects graphics.....	51
Appendix C. FTIR spectra for pyridine TPD recorded of the synthesized zeolites at 298, 373, 473 and 623 k.....	59
Appendix D. Conversion and selectivity of the alkylation of phenol with tert-butyl alcohol using the synthesized samples and the seed as catalyst.....	61

Abbreviations

SBU	Structural Building Unit
SDA	Structure Directing Agent
MOR	Mordenite
TBA	Tert-butyl alcohol
2,4-DTBP	2,4-di-tert-butyl-phenol
2-TBP	2-tert-butyl-phenol
3-TBP	3-tert-butyl-phenol
4-TBP	4-tert-butyl-phenol
t-BPE	Tert-butyl phenyl ether

Resumen

Título: Estudio del efecto de las variables de síntesis en las propiedades fisicoquímicas de una zeolita zsm-5 sintetizada mecano-químicamente*

Autor: Julieth Tatiana García Sánchez**

Palabras clave: ZSM-5, zeolita, semilla, libre de solvente, síntesis

Descripción:

La síntesis de zeolitas sin el uso de solventes y de agentes directores de estructuras orgánicas (OSDA) se ha convertido en una opción prometedora en los últimos años. Esta ruta permite una reducción en las emisiones de gases contaminantes (NOx) y un mejor uso de la energía del proceso. De cara al fortalecimiento en el conocimiento de esta ruta, son necesarios estudios que permitan correlacionar las variables de síntesis con las propiedades fisicoquímicas de los materiales finales. Sin embargo, hasta el momento no se han reportado estudios detallado sobre la influencia que ejercen las variables que intervienen en el proceso de molienda, sobre las características fisicoquímicas de los materiales.

Teniendo en cuenta lo mencionado anteriormente, el propósito de este trabajo fue estudiar el efecto de las condiciones de síntesis en la obtención de una zeolita ZSM-5 a través de una ruta libre de solventes mediante un enfoque mecano-químico. Se estudió el efecto del tiempo y la velocidad de molienda, la relación molar $\text{Na}_2\text{O}/\text{SiO}_2$ y la relación molar $\text{H}_2\text{O}/\text{SiO}_2$, las cuales fueron seleccionadas como variables clave para la síntesis de la zeolita. Los resultados mostraron que los dos primeros factores tuvieron un efecto positivo sobre las propiedades texturales, estructurales y la acidez de las zeolitas sintetizadas y que la relación $\text{H}_2\text{O}/\text{SiO}_2$ no tiene una influencia significativa sobre estas propiedades. Finalmente se evaluaron las propiedades catalíticas de las zeolitas sintetizadas y se compararon con una zeolita comercial. En general, esta contribución permite ampliar el conocimiento sobre este tipo de síntesis (libre de solvente y de SDAs) cuyas ventajas medioambientales y económicas pueden ser mayores a sus contrapartes convencionales.

*Trabajo de grado

**Facultad de Ingenierías Fisicoquímicas. Escuela de Ingeniería Química. Director: Prof. Víctor Gabriel Baldovino Medrano. Codirector: MSc. Iván Darío Mora Vergara.

Abstract

- Title:** A study on the effect of the synthesis variables of mechano-chemically synthesized zsm-5 on its physicochemical properties*
- Author:** Julieth Tatiana García Sánchez**
- Keywords:** ZSM-5, zeolite, seed, solvent-free, synthesis.
- Description:**

The synthesis of zeolites without the use of organic structure directing agent (OSDA) has become a promising option in recent years, this route allows a reduction in emissions of pollutant gases (NO_x) and a better use of process energy. With a view to strengthening the knowledge of this route, studies are needed to correlate the synthesis variables with the physicochemical properties of the final materials. However, no detailed studies on the influence of the variables involved in the milling process have been reported so far.

Given the above mentioned, the purpose of this work was to study the effect of the synthesis conditions in obtaining a ZSM-5 zeolite through a solvent-free route by a mechanochemical approach. The impact of the time and milling speed, the Na₂O/SiO₂ molar ratio, and the H₂O/SiO₂ molar ratio were studied, which were selected as key variables for zeolite synthesis. The results showed that the first two factors had a positive effect on the textural and structural properties and on the acidity of the synthesized zeolites, and H₂O/SiO₂ has a negligible effect on these properties. Finally, the catalytic properties of the synthesized zeolites were evaluated and compared with a commercial zeolite. In general, this contribution allows us to broaden our knowledge about this type of synthesis (solvent-free and SDA-free) whose environmental and economic advantages may be higher than its conventional counterparts.

*Bachelor Thesis

**Facultad de Ingenierías Físicoquímicas. Escuela de Ingeniería Química. Director: Prof. Víctor Gabriel Baldovino Medrano. Codirector: MSc. Iván Darío Mora Vergara.

Introduction

Zeolites are crystalline solids made of silicon, aluminium, and oxygen, which form structures with cavities and channels of different sizes. These materials are known for their high surface areas, strong acidity, large pore volumes, and high thermic and hydrothermal stability (Liu, Yang, Yan, Wang, & Zhou, 2019) (Wu Q. , y otros, 2014). Due to its electronic distribution, the aluminium present in the framework generates high-density negative charge regions, which are balanced by metal cations hence producing acid sites and making them useful in catalytic processes (Chassaing, Bénateau, & Pale, 2018) (Corregidor, Acosta, & Destéfanis, 2018). Until 2016, 232 zeolite structures were reported (IZA, 2016), among which those named as Y, A, X, L, and ZSM-5 stand out for their extensive use in industrial processes such as separation and adsorption (Ruren, Wenqin, Jihong, Qisheng, & Jiesheng, 2007) (Shirazi, Jamshidi, & Ghasemi, 2008). Besides, they are heavily used as catalysts in air and water pollution remediation, biomass conversion, and fuel production (Li, Li, & Yu, 2017).

The so-called ZSM-5 zeolite (Zeolite Socony Mobil-type 5) was first synthesized in 1972 (Patente nº 3,702,886, 1972). Figure 1 shows its structure. It consists of 10-member rings structure, figure 1a, composed of 5-member rings called pentasil units, figure 1b, which, when linked by hydrogen bonds, give rise to the structure of the material (Kokotailo, Lawton, Olson, & Meier, 1978) (Zoubida & Hichem, 2018). This zeolite presents a zig-zag shaped channels system with dimensions of 0.55 nm x 0.51 nm that intersect a straight channel of 0.56 nm x 0.53 nm giving rise to a three-dimensional porous network (Szostak, 1989) (Lei, Jockusch, Ottaviani, & Turro, 2003), figure 1c. These properties make ZSM-5 a zeolite with high shape selectivity towards small reaction products, since they diffuse faster through its three-dimensional network of pores

(Musilová, Žilková, Park, & Čejka, 2010). In addition, owing to its thermal stability, acidity, and porous structure, ZSM-5 is extensively used in petrochemistry (Khatamian & Irani, 2009).

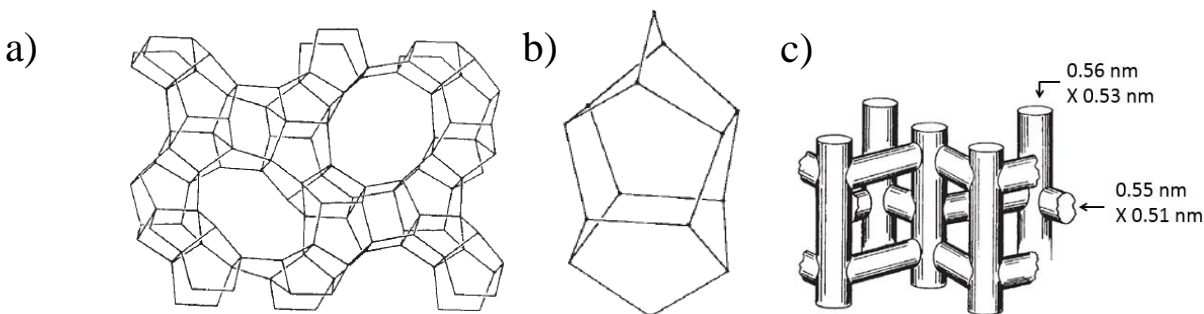


Figure 1. ZSM-5 zeolite, (a) zeolite structure, (b) pentasil units, (c) porous channels structure

(Kokotailo, Lawton, Olson, & Meier, 1978).

The ZSM-5 zeolite is synthesized in industry via the solvothermal route (Xu & Xu, *Modern Inorganic Synthetic Chemistry* (Second Edition), 2017). The latter requires the use of large amounts of solvents such as: water, alcohol or ionic liquids, as well as consuming important amounts of the so-called organic structure-directing agents (OSDA) which are usually toxic substances (Cooper, y otros, 2004). The synthesis process comprises a crystallization stage, in which the precursors of the crystals of the zeolite undergo a thermal treatment under high autogenous pressures. These conditions reduce the yield per reactor volume (Chen, Han, Cui, & Zhang, 2019) (Wu Q. , y otros, 2014) (Zhang, Li, & Bao, 2019). Subsequently, the organic structure-directing agents must be eliminated by thermal treatments such as roasting or calcination that generate polluting gases such as nitrogen oxides and carbon dioxide (Meng & Xiao, 2013).

An alternative to avoid the use of organic structure-directing agents is replacing them with zeolite seeds; i.e. small amounts of the zeolite to be synthesized. The seed is included in the mixture of the precursors of the material (Wu Q. , y otros, 2014). There have been reports on the success of this strategy for shortening the crystallization time of the zeolites and on improving the yields of the synthesis process (Fan, y otros, 2018). Furthermore, research has been made that

demonstrates the feasibility of both the solvent-free and organic template-free synthesis of zeolites (Ren , y otros, 2012) (Wu Q. , y otros, 2014) (Corregidor, Acosta, & Destéfanis, 2018) (Yue , y otros, 2018) (Wu, Meng , Gao, & Xiao, 2018). These works claim higher yields of zeolites, the use of lower reacting pressures during the crystallization stage, a decrease in gas emissions, lower energy expenses and lower production costs.

Although it has been possible to avoid the use of solvents Wu et al. (Wu, Meng , Gao, & Xiao, 2018) have formulated the hypothesis that water works as a "catalyst" during the synthesis and therefore, there should be a minimum amount of water involved in zeolite preparation. In general, the required solvent amount is obtained from the aluminium and silicon precursors hydration.

Considering the solvent-free synthesis of zeolites, this process involves three fundamental stages: mixing of the aluminium and silicon precursors with the structuring agent, milling, and crystallization (Wu, Meng , Gao, & Xiao, 2018). Some have considered that the milling stage serves to chemically activate the solid raw materials (Majano, Borchardt, Mitchell, Valtchev, & Pérez Ramírez, 2014). Most literature reports on the solvent-free synthesis of zeolites is based on milling with mortar and pestle. This strategy, although it is very easy to implement at the laboratory level is impractical and hardly reproducible. In fact, Biang et al. (Nada, Gillan, & Larsen , 2019) reported that changing the milling time in mortar and pestle procedures alters the structure of the zeolite to be synthesized. These authors (Nada, Gillan, & Larsen , 2019) also reported the zeolites produced by milling with mortar and pestle and a planetary ball mill were different. Therefore, this can mean that a change in the energy supplied during milling can affect the characteristics of the synthesized zeolite. It is also possible to quantify this energy as a function of time and the speed of the process when using a planetary ball mill (Khoa, Bae, Bae, Kim, & Kim, 2014).

Another important variable for the synthesis of ZSM-5 is the loading of sodium of the synthesis mixture. The amount of sodium is typically expressed in terms of the $\text{Na}_2\text{O}/\text{SiO}_2$ molar ratio (Dai,

Suzuki, Takahashi, & Saito, 1986). Chen et al. (Chen, Guan, Zhang, Wang, & Jiang, 2019) reported that a variation of the ratio $\text{Na}_2\text{O}/\text{SiO}_2$ molar ratio can lead to the formation of frameworks other than the MFI of ZSM-5; namely, mordenite, and, in some cases even amorphous quartz ($\alpha\text{-SiO}_2$). The presence of these phases also depends on the Si/Al molar ratio with which the ZSM-5 zeolite is synthesized. Therefore, both the amount of sodium and the Si/Al molar ratio must be considered when designing a synthesis process for ZSM-5.

The material produced after milling is further submitted to the crystallization stage in the same manner as in the conventional process. The conditions for this process vary depending on the characteristics of the targeted zeolite. For ZSM-5, crystallization is usually achieved by heating between 170°C and 180°C for 24 h. Conversely, when the process is assisted with ZSM-5 seeds, some reports indicate that crystallization can be achieved after 5 min, although, the temperature must be raised to 240°C (Bian, y otros, 2017). In general, crystallization assisted by organic structuring agents cannot be carried out at temperatures higher than 180°C due to the thermal decomposition of the agent. Consequently, longer crystallization times are required to compensate for the slower kinetics of the process.

Therefore, in order to scale-up the production of zeolites via this kind of methods, it is necessary to systematically study and define the effects of the variables that define the milling stage on the physicochemical properties of the zeolites thus synthesized. Taking into account the arguments presented so far, we decided to investigate the effects of the following synthesis variables in the production of ZSM-5 assisted by seeds: the milling time and speed of the milling stage as performed with a planetary ball mill, and the $\text{Na}_2\text{O}/\text{SiO}_2$ and $\text{H}_2\text{O}/\text{SiO}_2$ molar ratios. We assessed the effects of these variables on the chemical, textural, structural, and morphological properties of the synthesized materials. We also investigated the catalytic properties of the synthesized materials in the alkylation of phenol with tert-butyl alcohol (TBA) to produce butyl phenols since this is a

promising application of ZSM-5. In general, butyl phenols serve as raw materials for the production of antioxidants, phenolic resins, agrochemicals, printing inks, and fungicides (Nagose & Dukhande, 2017). Both the conversion and selectivity of this alkylation reaction depend on the acidity of the zeolite. More specifically, they are controlled by the nature and relative distribution of the acid sites since both Brønsted and Lewis acid sites are intrinsically reactive (Sakthivel, Dapurkar, Gupta, Kulshreshtha, & Selvam, 2003) (Shali, 2006). Figure 2 depicts the reaction scheme for the alkylation of phenol with TBA. Accordingly, the reaction allows for the production of tert-butyl phenyl ether (t-BPE), 2-tert-butyl-phenol (2-TBP), 4-tert-butyl-phenol (4-TBP), and 2,4-di-tert-butyl phenol (2,4-DTBP) (Jiang, y otros, 2015).

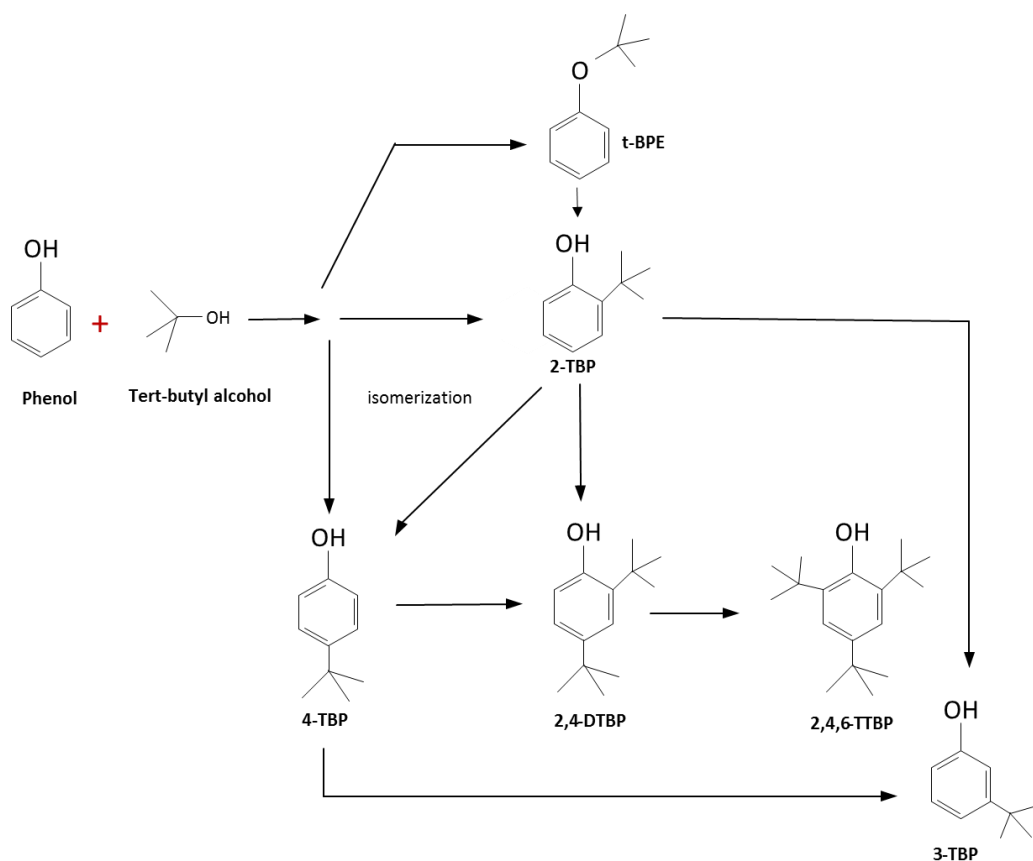


Figure 2. Phenol alkylation with tert-butyl alcohol using as a catalyst a ZSM-5 zeolite, reaction scheme (Jiang, y otros, 2015) (Adam, Hello, & Ali, 2011). tert-butyl phenyl ether (t-BPE), 2-tert-butyl-phenol (2-TBP), 4-tert-butyl-phenol (4-TBP), 3-tert-butyl-phenol (3-TBP), 2,4-di-tert-butyl phenol (2,4-DTBP) and 2,4,6-tri-tert-butyl phenol (2,4,6-TTBP)

1. Objectives

1.1 General objective

To study the effect of the synthesis variables on the physicochemical properties of ZSM-5 synthesized by a mechano-chemical route.

1.2. Specific objectives

- To assess the effects of the milling time, milling speed, and the $\text{Na}_2\text{O}/\text{SiO}_2$ and $\text{H}_2\text{O}/\text{SiO}_2$ molar ratios on key physicochemical properties of the materials.
- To evaluate the reactivity of the produced materials on the alkylation of phenol with tert-butyl alcohol.

2. Experimental section

The methodology of the work was divided in the three stages described in the following diagram, figure 3:

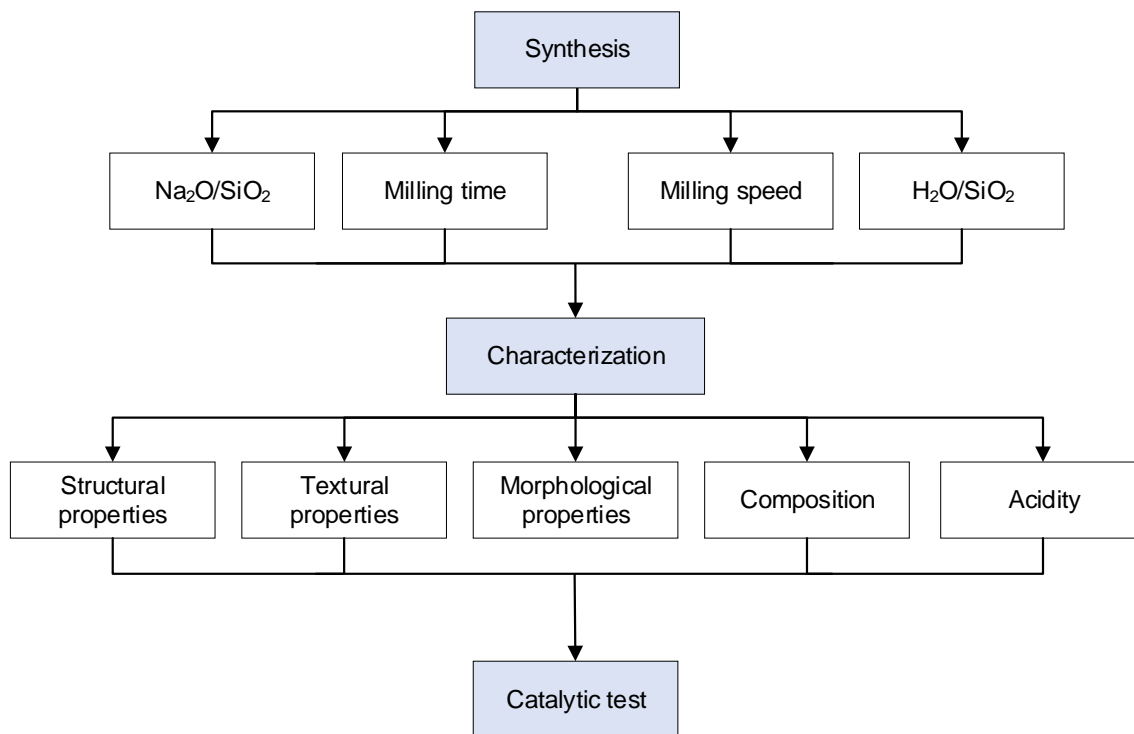


Figure 3. Methodological stages of the project

2.1 Materials synthesis

Fumed silica (SiO_2 0.007 μm , >99.9%, Aldrich) and hydrated sodium silicate ($\text{Na}_2\text{SiO}_3 \cdot 5\text{H}_2\text{O}$, >99.9%, Aldrich) were used as silicon precursors. $\text{Na}_2\text{SiO}_3 \cdot 5\text{H}_2\text{O}$ was also used as a source of sodium in conjunction with sodium hydroxide (NaOH , >99%, Merck). Hydrated aluminium sulfate ($\text{Al}_2(\text{SO}_4)_3 \cdot 18\text{H}_2\text{O}$ 97%, Merck) was used as aluminium source. Type I water was added by the hydration of the precursors and, if required, by an external source.

Milling was carried out in a planetary ball mill (Retsch-PM100) using a 125 mL stainless steel jar and 29 beads of 1 cm diameter. The precursors of silicon, aluminium, and sodium were mixed with a given amount of a commercial ZSM-5 zeolite (CBV 2314, Zeolyst International) used as seed. A Si/Al molar ratio of 13.23 and a seed/ SiO_2 weight ratio of 0.08 were maintained in all

cases. We designed a full factorial 2^4 experiment to study the effects of the selected synthesis variables following design featured in table 1. The experiments were executed in a randomized order as shown in table 2. For milling during 20 min, the rotation in the planetary ball mill was alternated between clockwise and anti-clockwise rotation allowing for 1 min stops between each type of rotation. This procedure was adopted to avoid sample overheating during operation. this in order not to overheat the mill and obtain more efficient grinding.

Table 1

Experimental design

Sample	A	B	C	D
1	-	-	-	-
2	-	-	-	+
3	-	-	+	-
4	-	-	+	+
5	-	+	-	-
6	-	+	-	+
7	-	+	+	-
8	-	+	+	+
9	+	-	-	-
10	+	-	-	+
11	+	-	+	-
12	+	-	+	+
13	+	+	-	-
14	+	+	-	+
15	+	+	+	-
16	+	+	+	+

Variables	-	+
A: Na ₂ O/SiO ₂ [mol/mol]	0.2	0.4
B: Milling time [min]	5	20
C: Milling speed [rpm]	200	400
D; H ₂ O/SiO ₂ [mol/mol]	1.7	2

The samples obtained after milling were put into a sealed autoclave where they were maintained under autogenous pressure while heating at 180°C for 24 h in a static oven. Afterwards, the autoclaves were cooled to room temperature putting them in cold water. The produced solids were recovered from the autoclaves and further washed with type I water and centrifuged for 15 min to remove any unreacted soluble precursors. The produced solids were named following the

nomenclature Z-Na#-T#-S#-H#, where Na corresponds to the Na₂O/SiO₂ molar ratio, T at the milling time, S at the milling speed and H at the H₂O/SiO₂ molar ratio.

Table 2

Order of execution of the experiments

Sample code	Order	Sample code	Order
Z-Na0.2-T5-S200-H1.7	16	Z-Na0.4-T5-S200-H1.7	12
Z-Na0.2-T5-S200-H2.0	13	Z-Na0.4-T5-S200-H2.0	14
Z-Na0.2-T5-S400-H1.7	2	Z-Na0.4-T5-S400-H1.7	1
Z-Na0.2-T5-S400-H2.0	3	Z-Na0.4-T5-S400-H2.0	6
Z-Na0.2-T20-S200-H1.7	4	Z-Na0.4-T20-S200-H1.7	9
Z-Na0.2-T20-S200-H2.0	11	Z-Na0.4-T20-S200-H2.0	5
Z-Na0.2-T20-S400-H1.7	7	Z-Na0.4-T20-S400-H1.7	8
Z-Na0.2-T20-S400-H2.0	10	Z-Na0.4-T20-S400-H2.0	15

2.2. Assessment of physicochemical properties

The morphology of the materials was observed from images collected with a QUANTA FEG 650 scanning electron microscope (FEI). Previous to the analyses, the samples were coated by gold sputtering.

The specific surface area and porosity of the materials were estimated after recording Argon adsorption-desorption isotherms at 87 K. Isotherms were recorded with a 3Flex apparatus (Micromeritics). For the analyses, samples of approximately 0.15 g of the materials were dried at 120 °C during 2h and overnight at 300 °C under vacuum. Specific surface areas were calculated with the BET method (Brunauer, Emmett, & Teller, 1938) after optimization of the CBET

parameter with the Rouquerol consistency criteria (Rouquerol, Llewellyn, & Rouquerol, 2007). Meanwhile, pore size distributions were estimated applying NLDFT cylindrical model. Adsorption-desorption isotherms were plotted taking into account the Chi (χ) theory where χ corresponds to $-\ln(-\ln(P/P_0))$ (Condon, 2006).

The chemical structure of the materials was analysed by infrared spectroscopy using a Nicolet iS50 Fourier Transform Infrared (FT-IR) spectrometer (ThermoScientific), equipped with attenuated total reflectance (ATR-FTIR). Crystallinity was measured by collecting X-ray diffraction (XRD) patterns with a D8 advance X-ray diffractometer (Bruker) provided with Cu K α 1 radiation. XRD patterns were recorded between 2θ angles of 3.5-70 with a 0.02 step size. To evaluate the relative crystallinity of the synthesized materials, the XRD pattern of the ZSM-5 seed was used as a reference and equation 1 was applied. It was assumed that the crystallinity of the seed is 100%. Besides, the percentage of the crystalline phases was determined using equation 2.

$$\%Crystallinity = \frac{\text{dominant peaks area of the sample}}{\text{dominant peaks area of the seed}} * 100 \quad (1)$$

$$\%Crystalline \text{ phase} = \frac{\text{dominant peaks area of the crystalline phase (MOR or ZSM - 5)} * 100}{\text{dominant peaks area of the ZSM - 5} + \text{dominant peaks area of the MOR}} \quad (2)$$

The acidity of the materials was evaluated by the FT-IR analysis of adsorbed pyridine using the experimental set-up described by (Carrillo & Cuello, 2017). Pyridine was adsorbed on self-supporting wafers of the solids at 150°C. The samples were evacuated in vacuum for 15 min at room temperature. Pyridine was desorbed from the samples at 100, 200, and 350°C. Before the tests, samples were heated at 400°C for 6h under vacuum to desorb any residual water or other contaminants from the atmosphere.

The relative concentration of acid sites, either Brønsted or Lewis, was determined using equations (3) and (4) (Emeis, 1993).

$$C_B = IA(B)\pi \frac{R^2}{W\epsilon} \quad (3)$$

$$C_L = IA(L)\pi \frac{R^2}{W\epsilon} \quad (4)$$

C_B : Brønsted acid sites concentration [mmol/g]

R : Radius of catalyst disk [cm]

C_L : Lewis acid sites concentration [mmol/g]

W : Weight of disk [mg]

$IA(B, L)$: Integrated absorbance of Brønsted or Lewis band (cm^{-1})

ϵ : Extinction coefficient [$\text{cm}/\mu\text{mol}$]. 1.67 for Brønsted and 2.22 for Lewis.

2.3. Catalytic tests

2.3.1. Catalysts activation. For the catalytic tests, the synthesized materials were activated by ion exchange of their Na^+ cations with a 1M ammonium nitrate solution (NH_4NO_3 >99%, PanReac). Such a procedure is mandatory to obtain the acidic zeolite. For the ion exchange, ca. 30 ml/g of zeolite were put in contact with NH_4NO_3 . The mixture was heated to 60°C and kept 16 h under magnetic stirring, and then washed twice. The procedure was repeated three times, and, subsequently, the sample was dried. Finally, the sample was calcined at 550°C , heating rate: $1.5^\circ\text{Cmin}^{-1}$, for 6h.

2.3.2. Reaction procedure. The alkylation of phenol with tert-butyl alcohol (TBA) was carried out in a 40 mL stainless steel high-pressure reactor with PTFE-lining. In a typical run, 69.1 mmol phenol ($\text{C}_6\text{H}_5\text{OH}$ 99%, Alfa Aesar), 69.1 mmol TBA ($\text{C}_4\text{H}_{10}\text{O}$ 99.5%, Aldrich), 0.25 g of catalyst, and 1.06 mmol dodecane ($\text{C}_{12}\text{H}_{26}$ >99%, Aldrich), used as an internal standard, were

mixed and put into the reactor. The mixture was heated to 120°C and kept 8h under magnetic stirring. The reaction proceeded under autogenous pressure, figure 4. After the reaction, the mixture was centrifugated and analyzed by gas chromatography using a GC (Agilent, HP 6890 GC) equipped with a flame ionization detector (FID) and a capillary column (HP-1, 100m×0.25mm×0.5µm). The identification of the reaction products was done by GC-MS analysis kindly provided by the laboratories of the Escuela de Ingeniería Química, UIS.

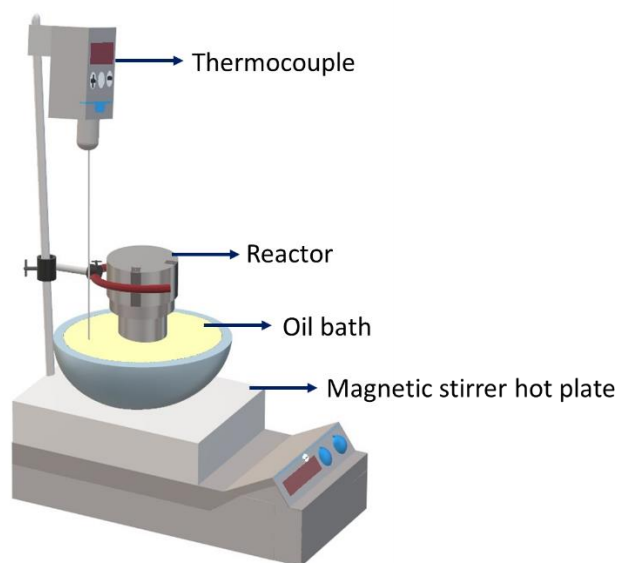


Figure 4. Experimental set-up for the test of alkylation of phenol with tert-butyl alcohol

3. Results and discussion

3.1. Materials properties

Eight out of the sixteen planned experiments resulted in the synthesis of solid materials. Indeed, all of the syntheses carried out with a $\text{Na}_2\text{O}/\text{SiO}_2=0.4$ resulted in the formation of a paste that

adhered firmly to the milling jar. The recovery of these materials was very hard. Such a fact showed the crucial role that sodium plays in the synthesis of ZSM-5. Considering these results, in what follows, we will focus on the analysis of the physicochemical properties of the eight solids produced with a $\text{Na}_2\text{O}/\text{SiO}_2=0.2$.

3.1.1. Morphology and chemical composition. Figure 5 shows SEM images of the commercial ZSM-5 zeolite used as a seed. We observed very fine particles whose shape mainly match cubic shaped crystals. The described morphology may be due to the low Si/Al ratio of the zeolite (Shirazi, Jamshidi, & Ghasemi, 2008). We also found rod shaped particles among the cubic crystals, figure 5b. These rods have also been observed for samples of mordenite zeolites (Zhang, y otros, 2011) hence showing that the seed contains mordenite as an impurity. We further verified the presence of mordenite in the seed by XRD, see Table 3.

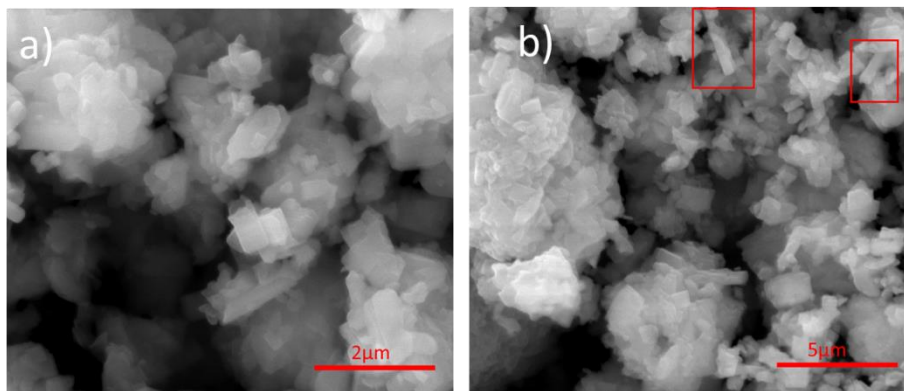


Figure 5. Micrographs of the seed (CBV 2314) with cubic shaped crystals and mordenite impurities with rod shapes.

Figure 6 shows SEM images for a selected sample before, figure 6a, and after, figure 6b, the crystallization stage. The powder recovered after ball milling did not show particles with a definite

shape. After the crystallization stage, well defined crystals were observed hence corroborating the fact that the mechano-chemical synthesis route is viable for producing zeolites (Wu Q. , y otros, 2014).

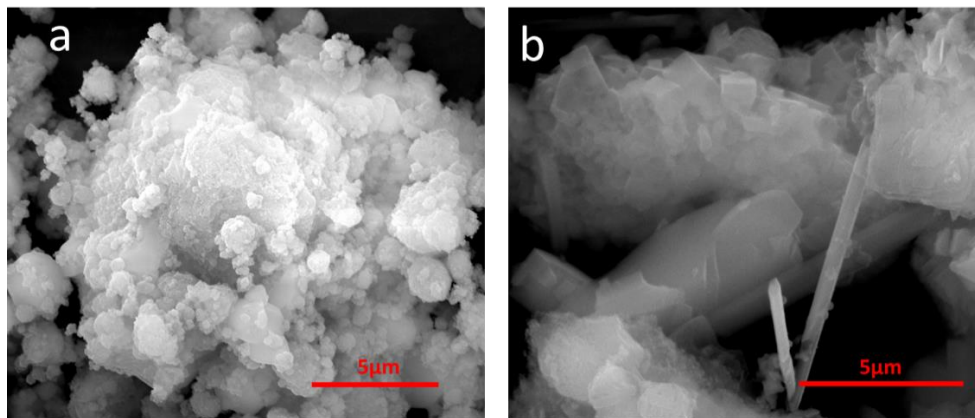


Figure 6. Effect of the crystallization on the morphological properties a) before crystallization (Z-t0) and b) after crystallization (Z-Na0.2-T5-S200-H1.7)

Figure 7 shows micrographs of the synthesized materials. The produced materials mainly showed cubic shaped crystals and rod-shaped particles that were similar to those of the ZSM-5 seed, figure 5. This finding showed that the implemented synthesis method led to the production of a material whose properties are similar to those of the seed. Indeed, XRD analysis showed that both the seed and the synthesized materials are composed of crystals of ZSM-5 and mordenite. In some cases, we also observed small orthorhombic crystals, which have also been reported for ZSM-5 zeolite (Caldeira, Santos, Pergher, Costa, & Araujo, 2016) (Perea, y otros, 2015). Literature explains that these crystals might be expected depending on how the crystallization stage of the zeolite is carried out (Zhang, y otros, 2011). In general, we found that the studied variations in the synthesis variables; milling time, milling speed, and the H_2O/SiO_2 ratio, did not produced strong

changes in the morphology of the synthesized solids. Figure 7 presents selected SEM images that illustrate this conclusion.

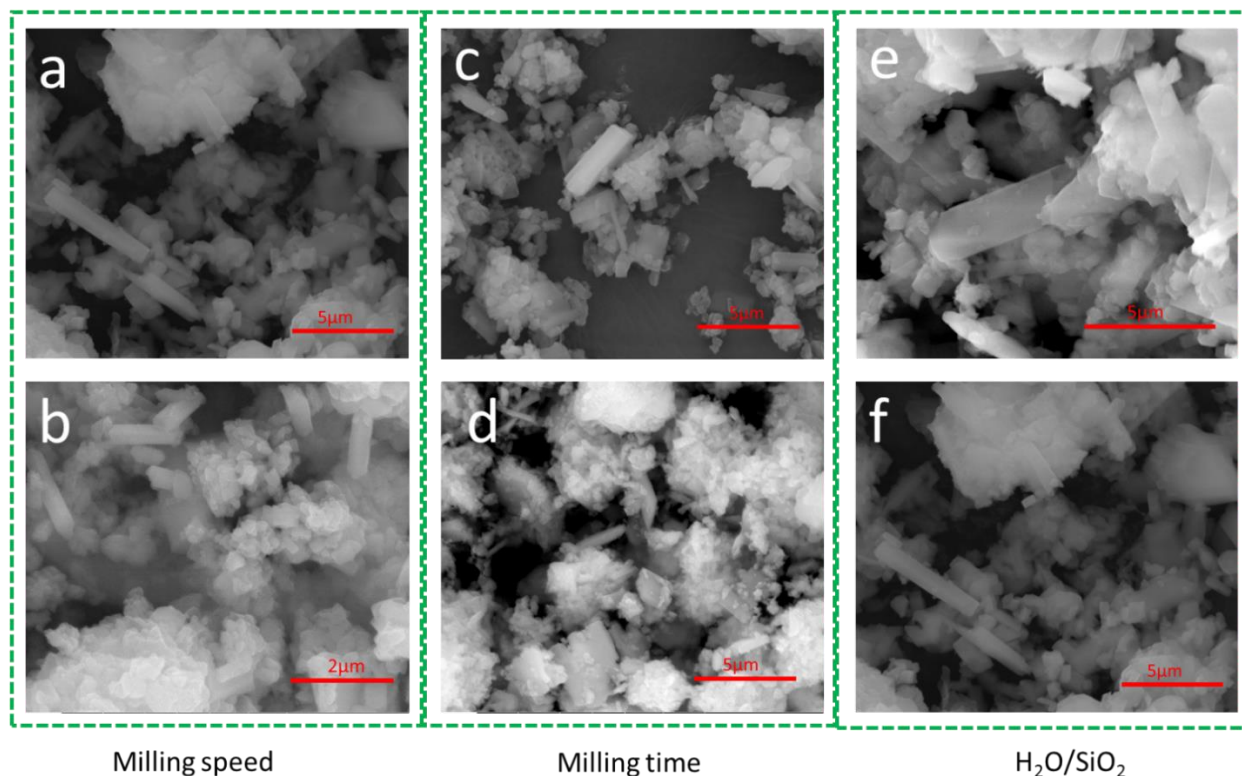


Figure 7. Selected SEM images for samples of the materials synthesized under the following conditions **a)** Z-Na_{0.2}-T₂₀-S₂₀₀-H_{2.0}, **b)** Z-Na_{0.2}-T₂₀-S₄₀₀-H_{2.0}, **c)** Z-Na_{0.2}-T₅-S₄₀₀-H_{1.7}, **d)** Z-Na_{0.2}-T₂₀-S₄₀₀-H_{1.7} **e)** Z-Na_{0.2}-T₂₀-S₂₀₀-H_{1.7} and **f)** Z-Na_{0.2}-T₂₀-S₂₀₀-H_{2.0}

Further SEM-EDS analyses of the studied samples was carried out for measuring the Si/Al ratio of the materials. Figure 8 shows the chemical composition of selected particles as measured by the aforementioned technique. In general, the samples showed a rather chemical homogeneous composition, see insets in figure 8. The Si/Al ratio of the samples was always larger than 8.0 with a maximum of 8.9 for the sample branded as Z-Na_{0.2}-T₅-S₂₀₀-H_{2.0}. The measured Si/Al ratios

were lower than the one measured for the ZSM-5 seed; Si/Al=10.3. Overall, these results are similar to those obtained when using seeds for the synthesis of zeolites by sol-gel (Ruren, Wenqin, Jihong, Qisheng, & Jiesheng, 2007) hence demonstrating that the mechano-chemical route may chemically proceed by a similar mechanism than the well-established ones in conventional processes.

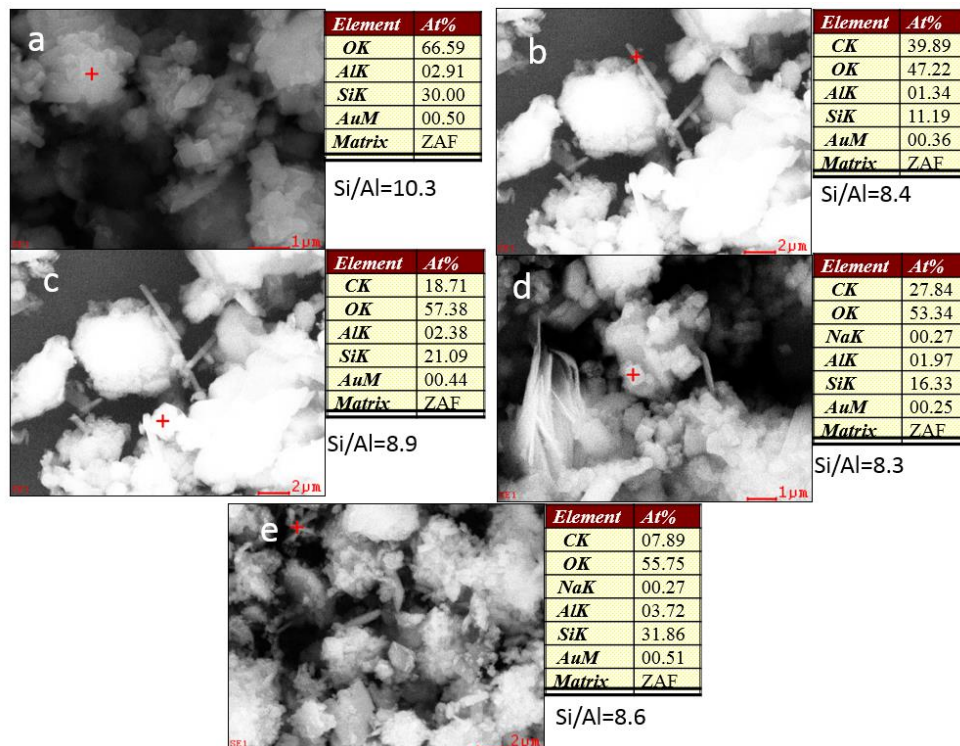


Figure 8. Molar composition and Si/Al ratio of samples synthesized under the following conditions: a) CBV 2314 b), c) Z-Na_{0.2}-T5-S200-H2.0 d) Z-Na_{0.2}-T5-S400- H1.7 and e) Z-Na_{0.2}-T20-S400-H1.7.

3.1.2. Materials crystallinity. Figure 9 shows the XRD patterns for samples of the materials after the crystallization stage. We also included the XRD pattern for a selected sample of the materials after ball milling for comparison purposes. Results show that no crystals are formed during ball milling as in agreement with the observations made from SEM. In general, the XRD

patterns of the materials resembled the one of the ZSM-5 seed. The production of ZSM-5 was further corroborated with the ATR-FTIR spectra of the synthesized materials, figure 10. We focus our discussion on the regions of the spectra around 550 cm^{-1} and 1210 cm^{-1} since the first region is associated to the detection of the five-member rings of the pentasil structural unit and the second to the asymmetric stretching of the tetrahedra of SiO_4 and AlO_4 in ZSM-5 (Xue, Wang, & He, 2012) (Cheng, Wang, Li, Yang, & Sun, 2005). As observed, these regions presented peaks attributable to the above-mentioned chemical structures hence validating the conclusion that it is possible to synthesize ZSM-5 via a mechano-chemical synthesis route. It is important to point out that these peaks are not found in the sample recovered after milling (Z-t0), as shown in figure 9a, which indicates that these characteristic ZSM-5 bands were not detected when analysing samples from the powders recovered after ball milling.

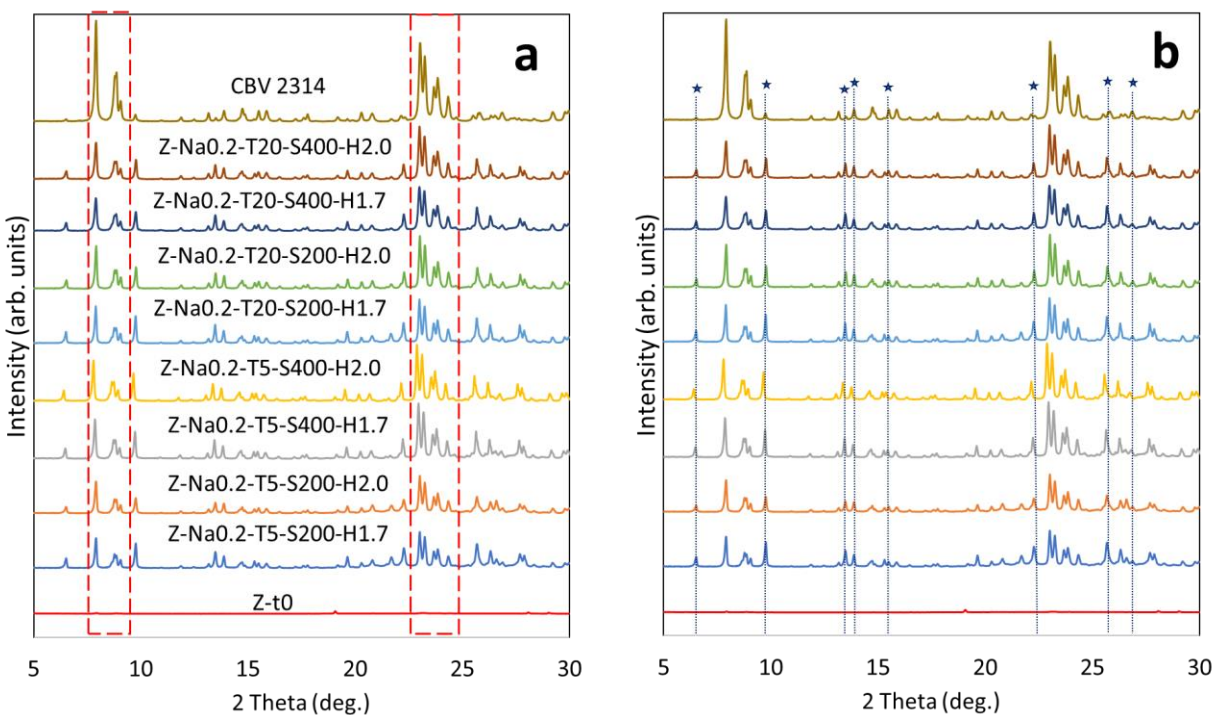


Figure 9. XRD patterns of synthesized zeolites a) ZSM-5 phase identification and b) mordenite phase impurity peaks.

As already mentioned, the employed ZSM-5 seed has a mordenite impurity. The presence of such an impurity was also observed for the materials synthesized by the mechano-chemical route, figure 9b. This illustrates how the seed acts a structure directing agent during the crystallization stage.

Table 3 displays the relative crystallinity of the synthesized materials including the relative percentages of both the ZSM-5 and mordenite phases. All samples of the synthesized materials had lower crystallinity as compared to the zeolite seed. The samples that had a higher crystallinity were those with a higher relative percentage of ZSM-5. Main effects plots from a statistical analysis of these results is presented in figure 11. These plots help elucidating the strength of the effects of the input variables on a selected response variable from a factorial experimental design (Montgomery, 1997) (Wu & Hamada, 2009). The conventional main effect plots were built adapting the method presented in a previous work from our research group (Caballero, Guerrero-Amaya, & Baldovino-Medrano, 2019). Particularly, our plots include the construction of a t-Student 95% confidence interval for the mean of the experiments.

In this case, we investigated how the milling speed, figure 11a, milling time, figure 11c, or the $\text{H}_2\text{O}/\text{SiO}_2$ molar ratio impacted the relative crystallinity of the materials when the $\text{Na}/\text{SiO}_2=0.2$ ratio. According to these plots, the milling speed had the strongest positive effect on the crystallinity of the materials while the effect of the milling time was negligible. On the other hand, the $\text{H}_2\text{O}/\text{SiO}_2$ molar ratio had a weak positive effect on crystallinity as evidenced by the fact that none of the averages of the relative crystallinity were near overcoming the limits of the 95% confidence interval for the mean of the crystallinity percentage. The conclusions from these plots were consistent with those of an analysis of variance, see appendix B. Furthermore, the latter was not able to detect effects from the interactions of the studied variables. One possible explanation

for these trends is that increasing the milling speed may favour the incorporation of sodium to the framework of the zeolite, hence promoting crystallization. It is known that sodium acts as a structure-directing agent during the synthesis of zeolites. However, its relative concentration must be carefully controlled since, for example, for ZSM-5, a high loading of sodium may promote the transformation of ZSM-5 into mordenite and into amorphous phases (Chen, Guan, Zhang, Wang, & Jiang, 2019). On the other hand, the negligible effect of the $\text{H}_2\text{O}/\text{SiO}_2$ molar ratio seems to confirm that water acts only as a catalytic agent during the crystallization stage of the process (Wu, Meng, Gao, & Xiao, 2018).

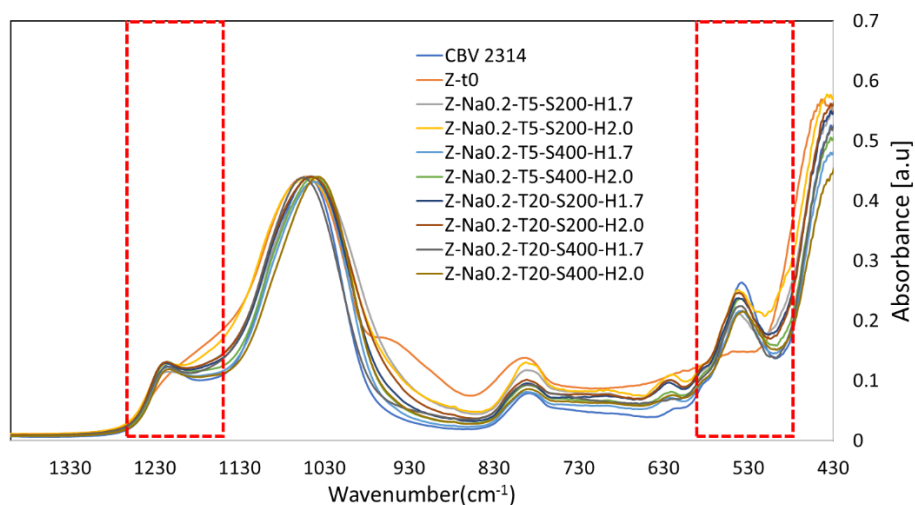


Figure 10. ATR-FTIR spectra with the presence of the characteristic bands of the ZSM-5 in the synthesized samples, the seed and the sample before the crystallization stage.

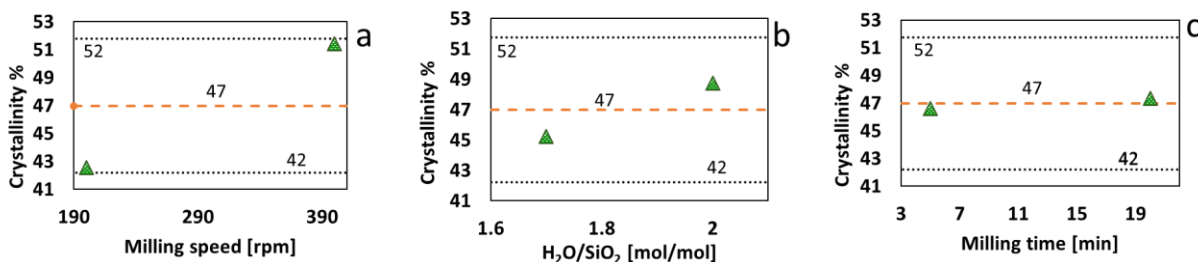


Figure 11. Main effects on the percentage of crystallinity of synthesized materials a) milling speed, b) H₂O/SiO₂ ratio and c) milling time. (-----) global average and (.....) confidence interval.

Table 3.

Crystallinity, ZSM-5 and mordenite percentage of the synthesized samples and the seed

Sample code	Crystallinity [%]	Mordenite [%]	ZSM-5 [%]
CBV 2314	100	7.5	92.5
Z-Na0.2-T5-S200-H1.7	39.4	49.2	50.8
Z-Na0.2-T5-S200-H2.0	40.9	40.6	59.4
Z-Na0.2-T5-S400-H1.7	52.7	36.9	63.1
Z-Na0.2-T5-S400-H2.0	53.5	38.3	61.7
Z-Na0.2-T20-S200-H1.7	41.7	47.7	52.3
Z-Na0.2-T20-S200-H2.0	48.2	39.6	60.4
Z-Na0.2-T20-S400-H1.7	47.1	44.1	55.9
Z-Na0.2-T20-S400-H2.0	52.5	34.3	65.7

3.1.3. Porosity and surface area. Figure 12 shows the Ar adsorption-desorption isotherms recorded for samples of synthesized materials based on the Chi theory (Condon, 2006). The isotherm of the ZSM-5 seed is also included for comparison purposes. Some samples exhibit slope changes that are associated with intraparticle voids observed by SEM analysis. On the other hand, all samples exhibited type I isotherms, as shown in Appendix A, characteristic of microporous materials (Reporting physisorption data for gas/solid systems with special reference to the

determination of surface area and porosity., 1982). The samples exhibited an apparent hysteresis loop that corresponds to the slope changes of figure 12.

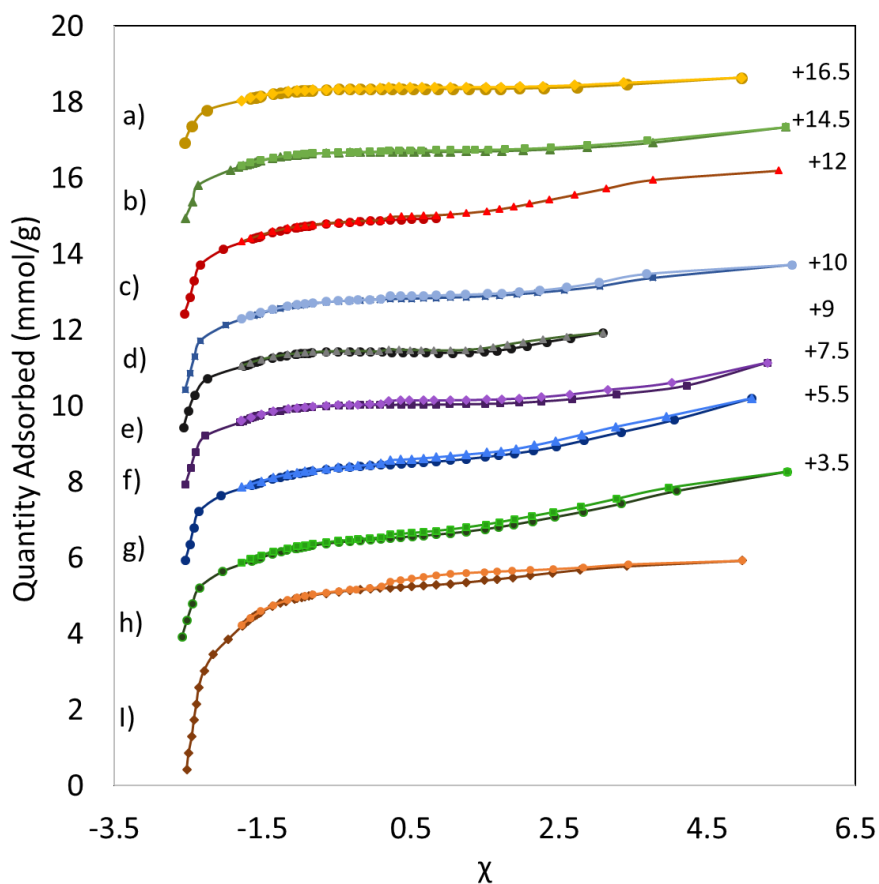


Figure 12. χ method Ar adsorption-desorption isotherms of the synthesized samples: **a)** Z-Na_{0.2}-T5-S200-H1.7, **b)** Z-Na_{0.2}-T5-S200-H2.0, **c)** Z-Na_{0.2}-T5-S400-H1.7, **d)** Z-Na_{0.2}-T5-S400-H2.0, **e)** Z-Na_{0.2}-T20-S200-H1.7, **f)** Z-Na_{0.2}-T20-S200-H2.0, **g)** Z-Na_{0.2}-T20-S400-H1.7, **h)** Z-Na_{0.2}-T5-S400-H2.0 and **i)** CBV 2314.

Table 4 summarizes the results obtained after performing calculations for determining the surface area and porosity of the materials. In general, the synthesized materials had lower surface area and pore volume than the ZSM-5 seed while keeping the average pore width of the latter.

Figure 13 shows main effects plots for the analysis of the effects of the milling rate, milling time, and the H₂O/SiO₂ ratio on the surface area of the materials. All of the input variables had positive effects on surface area. In general, the recorded trends are similar to these found when analysing the effects of the input variables on the crystallinity of the samples. This indicates that there is correlation between crystallinity and surface area. These conclusions are further supported by an ANOVA test, Appendix B.

Table 4

Synthesized materials properties

Sample code	S _{BET} [m ² /g]	S _{micro} [m ² /g]	S _{ext} [m ² /g]	V _{total} [cm ³ /g]	V _{micro} [cm ³ /g]	Average pore width [nm]
CBV 2314	407	369	39	0.192	0.129	0.58
Z-Na0.2-T5-S200-H1.7	148	138	10	0.056	0.047	0.58
Z-Na0.2-T5-S200-H2.0	174	161	13	0.077	0.056	0.58
Z-Na0.2-T5-S400-H1.7	221	195	27	0.120	0.069	0.58
Z-Na0.2-T5-S400-H2.0	218	194	24	0.108	0.068	0.58
Z-Na0.2-T20-S200-H1.7	194	184	10	0.082	0.064	0.58
Z-Na0.2-T20-S200-H2.0	201	185	15	0.087	0.065	0.58
Z-Na0.2-T20-S400-H1.7	222	189	33	0.122	0.062	0.58
Z-Na0.2-T20-S400-H2.0	225	190	35	0.127	0.067	0.58

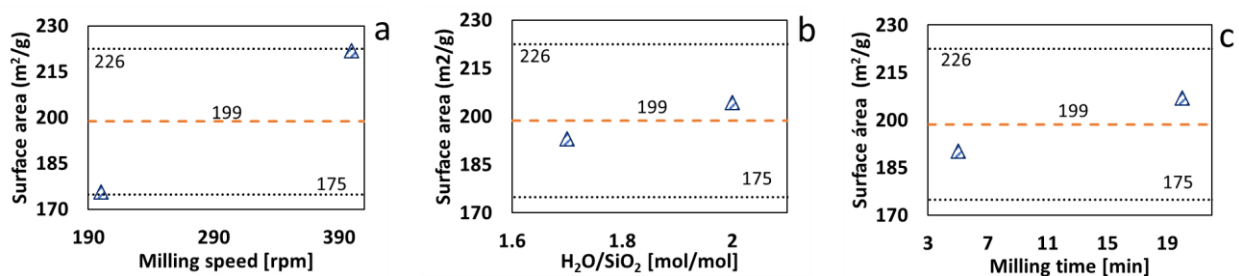


Figure 13. Main effects on the surface area of synthesized materials a) milling speed, b) H₂O/SiO₂ and c) milling time. (- - - -) global average and (.....) confidence interval.

3.1.4. Acidity of the materials. Figure 14 shows FTIR spectra recorded during the temperature programmed desorption (TPD) of pyridine. Therein, the bands at 1545 and 1455 cm^{-1} correspond to the adsorption of the probe molecule on Brønsted and Lewis acid sites, respectively. On the other hand, the band at 1491 cm^{-1} corresponds to an overlap of the signals from pyridine adsorbed on both the Brønsted and the Lewis sites. Finally, the band found at 1445 cm^{-1} corresponds to the physically adsorbed pyridine (Buzzoni, Bordiga, Ricchiardi, Lamberti, & Zecchina, 1996). The latter is of little interest since it does not account for the catalytic performance of the material. According to the results for the ZSM-5 seed, an increase in temperature promotes pyridine desorption mostly from Lewis sites. Indeed, the band associated to Brønsted sites barely decreased under the current conditions. Therefore, the ZSM-5 seed has strong Brønsted acidity. Appendix C shows the FTIR spectra for pyridine TPD recorded of the synthesized samples. The spectra are like those of the seed; namely, the synthesized materials also have strong Brønsted acidity. However, some samples also exhibited weak or mildly strong acid sites.

Table 5 shows the results of the calculations made to determine the total acidity of the materials as well as the concentrations of Brønsted and Lewis sites. As foreseen from the FT-IR spectra, the surface of the materials is mainly populated by Brønsted sites; which are due to the presence of H^+ protons in the zeolite structure after ionic-exchange. Figure 15 shows main effect plots for assessing the effects of the studied input variables on the total acidity of the materials. Both the milling speed and milling time had relatively strong positive effects on total acidity. These effects could be ascribed to an enhancement of the amount of Na^+ in the structure of the zeolite since Na^+ cations are exchanged with protons during the ion exchange process (Ruren, Wenqin, Jihong, Qisheng, & Jiesheng, 2007). On the other hand, the $\text{H}_2\text{O}/\text{SiO}_2$ ratio had the weakest effect on total acidity similar to surface area and crystallinity.

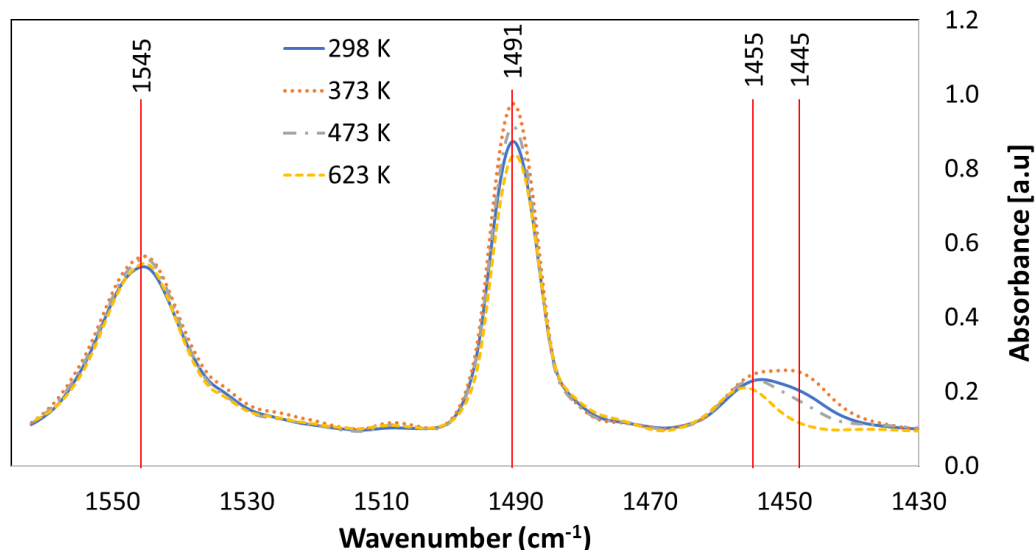


Figure 14. FTIR spectra for pyridine TPD recorded of CBV 2314 at 298, 373, 473 and 623 K. The highlighted bands correspond to pyridine adsorption on Brønsted (1545 cm^{-1}) and Lewis sites (1455 cm^{-1}). Band at 1491 cm^{-1} corresponds to an overlap of the signals from pyridine adsorbed on both the Brønsted and the Lewis sites and the band found at 1445 cm^{-1} corresponds to the physically adsorbed pyridine (Buzzoni, Bordiga, Ricchiardi, Lamberti, & Zecchina, 1996).

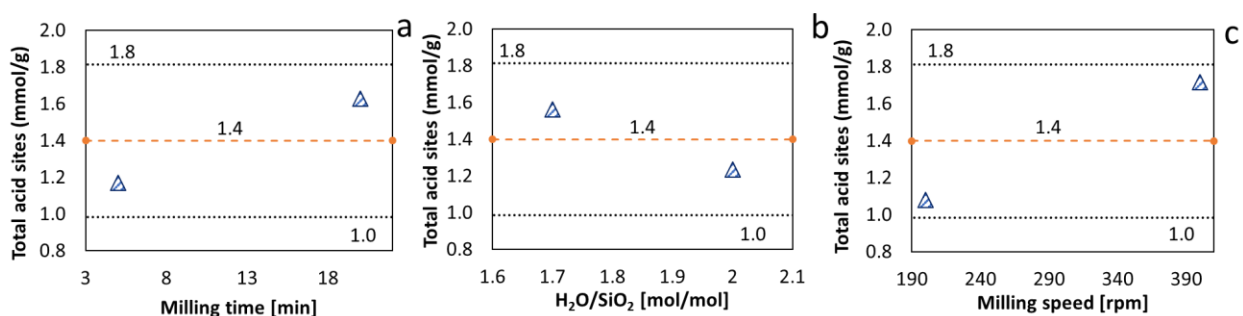


Figure 15. Main effects on the total acid sites concentration of synthesized materials a) milling time, b) $\text{H}_2\text{O}/\text{SiO}_2$ and c) milling speed. (- - - -) global average and (.....) confidence interval.

Table 5.

Concentration of total acid sites and of the Brønsted and Lewis sites for the synthesized samples and the seed, according to pyridine TPD test. [mmol/g]

Sample code	Concentration of acid sites [mmol/g]		
	Total	Brønsted	Lewis
CBV 2314	2.87	2.33	0.54
Z-Na0.2-T5-V200-H1.7	1.15	1.12	0.03
Z-Na0.2-T5-V200-H2.0	0.36	0.34	0.01
Z-Na0.2-T5-V400-H1.7	1.81	1.56	0.25
Z-Na0.2-T5-V400-H2.0	1.37	1.32	0.05
Z-Na0.2-T20-V200-H1.7	1.44	1.38	0.06
Z-Na0.2-T20-V200-H2.0	1.38	1.34	0.03
Z-Na0.2-T20-V400-H1.7	1.86	1.77	0.09
Z-Na0.2-T20-V400-H2.0	1.84	1.77	0.07

3.2. Catalytic performance

Table 6 shows the conversion and selectivity of the different materials during the reaction of alkylation of phenol with tert-butyl alcohol. Conversions were between 0.7 and 4.9%, which means that between 1.7 and 11.7 mmol of phenol were converted per gram of catalyst. These values were consistent with those reported in the literature when using ZSM-5 as a catalyst (Chen, Xue, Wu, & Wu, 2018). A more detailed description of the catalytic results is presented in Appendix D.

Figure 16 shows main effect plots for assessing the effects of the studied input variables on the phenol conversion. The observed trends are in strong correspondence with those already commented for the effects of these variables on the acidity of the materials. Namely, both the milling speed and milling time have strong positive effects on the catalytic conversion of phenol while the H₂O/SiO₂ ratio had a weaker but negative effect on the catalysis. Concerning selectivity, the main reaction product was tert-butyl phenyl ether, table 6. This may be because the

etherification process through which tert-butyl phenyl ether is produced requires less activation energy as compared to the other parallel reactions (Adam, Hello, & Ali, 2011).

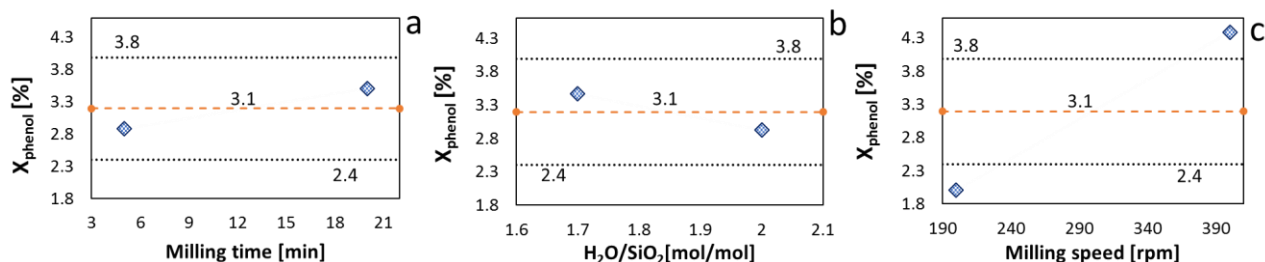


Figure 16. Main effects on phenol conversion a) milling time, b) $\text{H}_2\text{O}/\text{SiO}_2$ and c) milling speed.

(- - - - -) global average and (.....) confidence interval.

Table 6

Conversion and selectivity of the phenol alkylation with tert-butyl alcohol for each synthesized zeolite and the seed.

Sample	X_{Phenol}	%error	Selectivity of products (%)				
			2-TBP	4-TBP	3-TBP	2,4-DTBP	t-BPE
CBV 2314	3.8	3.2	5.5	4.7	0.4	0.1	89.4
Z-Na0.2-T5-V200-H1.7	2.7	24.5	2.6	3.0	0.1	0.1	94.3
Z-Na0.2-T5-V200-H2.0	0.7	14.8	1.9	2.1	0.1	0.0	95.8
Z-Na0.2-T5-V400-H1.7	4.3	10.1	3.0	3.4	0.2	0.0	93.3
Z-Na0.2-T5-V400-H2.0	3.8	29.5	7.2	5.9	0.5	0.1	86.3
Z-Na0.2-T20-V200-H1.7	2.2	22.5	4.7	4.8	0.3	0.0	90.1
Z-Na0.2-T20-V200-H2.0	2.3	8.9	2.8	2.5	0.1	0.0	94.6
Z-Na0.2-T20-V400-H1.7	4.7	6.3	16.1	13.4	1.1	0.4	69.0
Z-Na0.2-T20-V400-H2.0	4.8	19.3	7.9	8.3	0.6	0.1	83.0

4. Conclusions

The effect of milling speed, milling time and molar ratios of $\text{Na}_2\text{O}/\text{SiO}_2$ and $\text{H}_2\text{O}/\text{SiO}_2$ on the physicochemical properties of ZSM-5 zeolites synthesized through a mechano-chemical pathway was investigated. Under the studied conditions, an increase in the milling speed and time improved the surface area, crystallinity and acidity of the materials. Among the studied variables, the milling speed had the strongest effect on all the above mentioned properties. Conversely, the effect of $\text{H}_2\text{O}/\text{SiO}_2$ molar ratio on these properties was basically negligible. On the other hand, a high $\text{Na}_2\text{O}/\text{SiO}_2$ molar ratio (0.4) prevented the synthesis of zeolitic materials under the proposed conditions. In reference to the morphology of the materials, the synthesis variables studied did not generate a significant change.

The increase in milling energy (time and speed) generates an increase in both the acidity of the materials and their textural properties, which is reflected in a greater catalytic activity.

5. Recommendations

- To study the effect of the $\text{Na}_2\text{O}/\text{SiO}_2$ molar ratio at levels lower than those used in this work, to determine if it is possible to eliminate mordenite impurity from synthesized materials.
- To Carry out a kinetic study in the crystallization stage that allows to determine at what point the impurity begins to form and study how this crystallization time influences the material properties.
- To Carry out a study of diffusional limitations in the phenol alkylation reaction to improve the understanding of the phenomena associated with the reactivity of catalysts in this reaction.

6. Participation in events

This project participated in the poster modality at the 19th international zeolite conference in Perth, Australia (19th IZC). It was presented in the oral presentation modality at the XI Colombian Symposium on Catalysis (SiCCat 2019) in Popayan, Cauca and the X International Congress of Materials (CIM 2019) held at the Industrial University of Santander.

References

- Adam, F., Hello, K., & Ali, T. (2011). Solvent free liquid-phase alkylation of phenol over solid sulfanilic acid catalyst. *Applied Catalyst A: General*, 399, 42-49.
- Ali, M., Brisdon, B., & Thomas, W. (2003). Synthesis, characterization and catalytic activity of ZSM-5 zeolites having variable silicon-to-aluminum ratios. *Applied catalysis*, 252, 149-162.
- Argauer, R., & Landolt, G. (1972). *Patente n° 3,702,886*.
- Bian, C., Zhang, C., Pan, S., Chen, F., Zhang, W., Meng, X., . . . Xiao, F.-S. (2017). Generalized high-temperature synthesis of zeolite catalysts with unpredictably high space-time yields (STYs). *Journal of Materials Chemistry A*.
- Brunauer, S., Emmett, P., & Teller, E. (1938). Adsorption of gases in multimolecular layers. *Journal of the American Chemical Society*, 60(2), 309-312.
- Buzzoni, R., Bordiga, S., Ricchiardi, G., Lamberti, C., & Zecchina, A. (1996). Interaction of Pyridine with Acidic (H-ZSM5, H- β , H-MORD Zeolites) and Superacidic (H-Nafion Membrane) Systems: An IR Investigation. *Langmuir*, 12, 930-940.
- Caballero, K., Guerrero-Amaya, H., & Baldovino-Medrano, V. (2019). Revisiting glycerol esterification with acetic acid over Amberlyst-35 via statistically designed experiments: Overcoming transport limitations. *Chemical Engineering Science*, 207, 91-104.
- Caldeira, V., Santos, A., Pergher, S., Costa, M., & Araujo, A. (2016). Use of a low-cost template-free ZSM-5 for atmospheric petroleum residue pyrolysis. *Química Nova*, 39(3), 292-297.
- Carrillo, J., & Cuello, F. (2017). Implementación de una metodología para la medición de la acidez de catalizadores por análisis FTIR de piridina adsorbida en el ICP y transferencia tecnológica de esta técnica al CICAT-UIS. Bucaramanga, Colombia.

Chassaing, S., Bénétiau, V., & Pale, P. (2018). Green Catalysts based on Zeolites for Heterocycle Synthesis. *Current Opinion in Green and Sustainable Chemistry*, 10, 35-39.

Chen, L., Xue, T., Wu, H., & Wu, P. (2018). Hierarchical ZSM-5 nanocrystal aggregates: seed-induced green synthesis and its application in alkylation of phenol with tert-butanol†. *RSC Advances*, 8, 2751-2758.

Chen, S., Guan, D., Zhang, Y., Wang, Z., & Jiang, N. (2019). Composition and kinetic study on template- and solvent-free synthesis of ZSM-5 using leached illite clay. *Microporous and Mesoporous Materials*, 285, 170-177.

Chen, Y.-H., Han, D.-M., Cui, H.-X., & Zhang, Q. (2019). Synthesis of ZSM-5 via organotemplate-free and dry gel conversion method: Investigating the effects of experimental parameters. *Journal of Solid State Chemistry*, 279.

Cheng, Y., Wang, L.-J., Li, J. S., Yang, Y. C., & Sun, X. Y. (2005). Preparation and characterization of nanosized ZSM-5 zeolites in the absence of organic template. *Materials Letters*, 59, 3427-3430.

Condon, J. (2006). *Surface area and porosity determinations by physisorption: Measurements and Theory*. Elsevier.

Cooper, E., Andrews, C., Wheatley, P., Webb, P., Wormald, P., & Morris, R. (2004). Ionic liquids and eutectic mixtures as solvent and template in synthesis of zeolite analogues. *Nature*, 1012-1016. doi:10.1038/nature02860

Corregidor, P., Acosta, D., & Destéfanis, H. (2018). Kinetic study of seed-assisted crystallization of ZSM-5 zeolite in an OSDA-free system using a natural aluminosilicate as starting source. *Industrial & Engineering Chemistry Research*, 57, 13713-13720.

Cundy, C., & Paul, C. (2005). The hydrothermal synthesis of zeolites: Precursors, intermediates and reaction mechanism. *Microporous and mesoporous materials*, 82, 1-78.

Dai, F., Suzuki, M., Takahashi, H., & Saito, Y. (1986). Mechanism of Zeolite Crystallization without Using Template Reagents of Organic Bases. *Studies in Surface Science and Catalysis*, 28, 223-230.

Emeis, C. (1993). Determination of integrated molar extinction coefficients for infrared absorption bands of pyridine adsorbed on solid acid catalysts. *Journal of catalysis*, 141, 347-354.

Fan, C., Wang, Y., Li, H., Wang, X., Sun, C., Zhang, X., . . . Wang, S. (2018). Seed-induced synthesis of multilamellar ZSM-5 nanosheets directed by amphiphilic organosilane. *New Journal of Chemistry*, 42, 17043-17055.

IZA. (1 de October de 2016). *International Zeolite Association Database*. Obtenido de <http://www.iza-structure.org/DatabaseHistory.htm>

Jiang, T., Lu, L., Le, S., Ma, Y., Dai, L., Zhao, H., & Zhao, Q. (2015). Improvement of the catalytic activity of MCM-48 synthesized from metakaolinite in the alkylation of phenol with tert-butyl alcohol. *Applied Clay Science*, 109-110.

Khatamian, M., & Irani, M. (2009). Preparation and Characterization of Nanosized ZSM-5 Zeolite Using Kaolin and Investigation of Kaolin Content, Crystallization Time and Temperature Changes on the Size and Crystallinity of Products. *Journal of the Iranian Chemical Society*, 6, 187-194.

Khoa, H., Bae, S., Bae, S., Kim, B.-w., & Kim, J. S. (2014). Planetary Ball Mill Process in Aspect of Milling Energy. *Journal of Korean Powder Metallurgy Institute*, 21, 155-164.

Kim, S. D., Noh, S. H., Seong, K. H., & Kim, W. J. (2004). Compositional and kinetic study on the rapid crystallization of ZSM-5 in the absence of organic template under stirring. *Microporous and Mesoporous*, 72, 185-192.

Kokotailo, G., Lawton, S., Olson, D., & Meier, W. (1978). Structure of synthetic zeolite ZSM-5. *Nature*, 272, 437-438.

- Lei, X.-g., Jockusch, S., Ottaviani, M., & Turro, N. (2003). In situ EPR investigation of the addition of persistent benzyl radicals to acrylates on ZSM-5 zeolites. Direct spectroscopic detection of the initial steps in a supramolecular photopolymerization. *Photochemical & Photobiological Science*, 2, 1095-1100.
- Li, Y., Li, L., & Yu, J. (2017). Applications of Zeolites in Sustainable Chemistry. *Chem*, 3, 928-949.
- Liu, Y., Yang, X., Yan, C., Wang, H., & Zhou, S. (2019). Solvent-free synthesis of zeolite LTA monolith with hierarchically porous structure from metakaolin. *Material Letters*, 248, 28-31.
- Majano, G., Borchardt, L., Mitchell, S., Valtchev, V., & Pérez Ramírez, J. (2014). Rediscovering zeolite mechanochemistry – A pathway beyond current synthesis and modification boundaries. *Microporous and Mesoporous Materials*, 194, 106-114.
- Meng, X., & Xiao, F.-S. (2013). Green Routes for Synthesis of Zeolites. *Chemical Reviews*, 114, 1521-1543.
- Montgomery, D. (1997). *Design and analysis of experiments* (5 edition ed.). Arizona: John Wiley and Sons, Inc.
- Musilová, Z., Žilková, N., Park, S.-E., & Čejka, J. (2010). Aromatic Transformations Over Mesoporous ZSM-5: Advantages and Disadvantages. *Topics in Catalysis*, 53, 1457-1469.
- Nada, M., Gillan, E., & Larsen, S. (2019). Mechanochemical reaction pathways in solvent-free synthesis of ZSM-5. *Microporous and Mesoporous Materials*, 276, 23-28.
- Nagose, N., & Dukhande, V. (2017). Alkylation of Phenol with Tert-butyl Alcohol using (1-(4-sulfonic acid) butyl triethylammonium p-toulene sulfonic acid [SBTEA][PTSA]. *International Journal of Advance Research in Science and Engineering*, 6(4), 178-184.

Perea, D., Arslan, I., Liu, J., Ristanovic, Z., Koravik, L., Arey, B., . . . Weckhuysen, B. (2015). Determining the location and nearest neighbours of aluminium in zeolites with atom probe tomography. *Nature Communications*, 6(7589).

Ren, L., Wu, Q., Yang, C., Zhu, L., Li, C., Zhang, P., . . . Xiao, F.-S. (2012). Solvent-free synthesis of zeolites from solid raw materials. *Journal of the American Chemical Society*, 15173-15176.

Reporting physisorption data for gas/solid systems with special reference to the determination of surface area and porosity. (1982). *Pure & Applied Chemistry*, 54(11), 2201-2218.

Rouquerol, J., Llewellyn, P., & Rouquerol, F. (2007). Is the BET equation applicable to microporous adsorbents? *Studies in Surface Science and Catalysis*, 160, 49-56.

Ruren, X., Wenqin, P., Jihong, Y., Qisheng, H., & Jiesheng, C. (2007). *Chemistry of zeolites and related porous materials: Synthesis and structure*. John Wiley & Sons (Asia).

Sakthivel, A., Dapurkar, S., Gupta, N., Kulshreshtha, S., & Selvam, P. (2003). The influence of aluminium sources on the acidic behaviour as well as on the catalytic activity of mesoporous H-AlMCM-41 molecular sieves. *Microporous and Mesoporous Materials*, 65, 177-187.

Shali, N. (2006). Transition metal and rare earth metal modified sol-gel titania: a versatile catalyst for organic transformation. *PhD in Chemistry Thesis*, 178-196. Kerala, India: Cochin University of Science and Technology.

Shirazi, L., Jamshidi, E., & Ghasemi, M. (2008). The effect of Si/Al ratio of ZSM-5 zeolite on its morphology, acidity and crystal size. *Crystal Research and Technology*, 43(12), 1300-1306.

Squillace, P., Pankow, J., Korteş, N., & Zogorski, J. (1997). Review of the environmental behavior and fate of methyl tert-butyl ether. *Environmental Toxicology and Chemistry*, 16(9), 1836-1844.

Stach, H., Janchen, J., Jerschke, H.-G., Lohse, U., & Parltitz, B. (1992). Mordenite Acidity: Dependence on the Si/Al ratio and the framework aluminium topology. 2. Acidity Investigations. *Journal of Physical Chemistry*, 96, 8480-8485.

Szostak, R. (1989). *Molecular Sieves: Principles of Synthesis and Identification*. New York: Van Nostrand Reinhold.

Wu, Q., Wang, X., Qi, G., Guo, Q., Pan, S., Meng, X., . . . Xiao, F.-S. (2014). Sustainable Synthesis of Zeolites without Addition of Both Organotemplates and Solvents. *Journal of the American Chemical Society*, *136*, 4019-4025. doi:10.1021/ja500098j

Wu, J., & Hamada, M. (2009). *Experiments: Planning, Analysis, and Optimization, 2nd edition*. Wiley.

Wu, Q., Meng, X., Gao, X., & Xiao, F.-S. (2018). Solvent-Free Synthesis of Zeolites: Mechanism and Utility. *Accounts of Chemical Research*, *51*, 1396–1403.

Wu, Q., Wang, X., Qi, G., Guo, Q., Pan, S., Meng, X., . . . Xiao, F.-S. (2014). Sustainable Synthesis of Zeolites without Addition of Both Organotemplates and Solvents. *Journal of the American Chemical Society*, 4019-4025.

Xu, R., & Xu, Y. (2017). *Modern Inorganic Synthetic Chemistry (Second Edition)*. Elsevier.

Xu, R., Pang, W., Yu, J., Huo, Q., & Chen, J. (2007). *Chemistry of zeolites and related porous materials: synthesis and structure*. John Wiley & Sons (Asia).

Xue, T., Wang, Y., & He, M.-Y. (2012). Facile synthesis of nano-sized NH₄-ZSM-5 zeolites. *Microporous and mesoporous materials*, *156*, 29-35.

Yue, Y., Kang, Y., Bai, Y., Gu, L., Liu, H., Bao, J., . . . Bao, X. (2018). Seed-assisted, template-free synthesis of ZSM-5 zeolite from natural aluminosilicate minerals. *Applied Clay Science*, *158*, 177-185.

Zhang, C., Li, S., & Bao, S. (2019). Sustainable Synthesis of ZSM-5 Zeolite from Rice Husk Ash Without Addition of Solvents. *Waste and Biomass Valorization*, *10*, 2825-2835.

Zhang, L., Xie, S., Xin, W., Xiujie, L., Shenglin, L., & Xu, L. (2011). Crystallization and morphology of mordenite zeolite influenced by various parameters in organic-free synthesis.

Materials Research Bulletin, 46, 894-900.

Zoubida, L., & Hichem, B. (2018). The Nanostructure Zeolites MFI-Type ZSM5. En *Nanocrystals and Nanostructures* (págs. 43-60). Algeria.

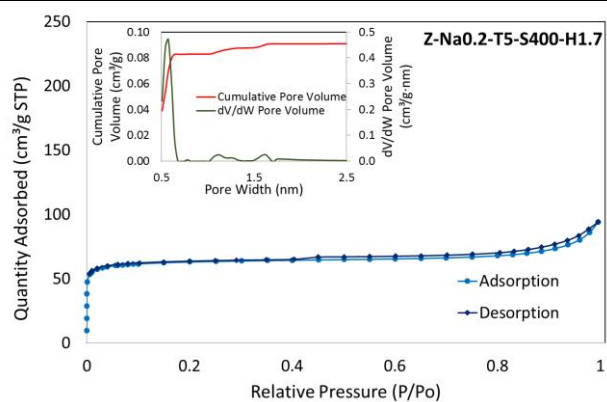
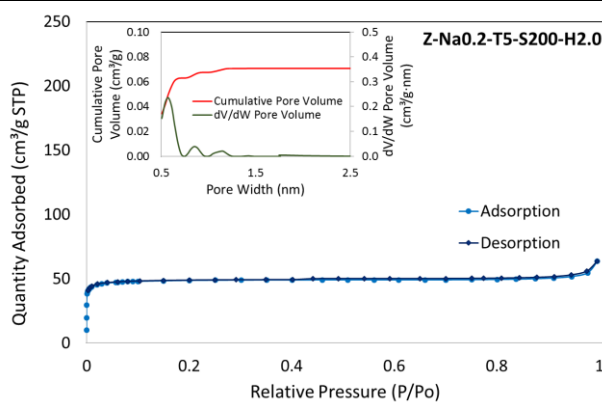
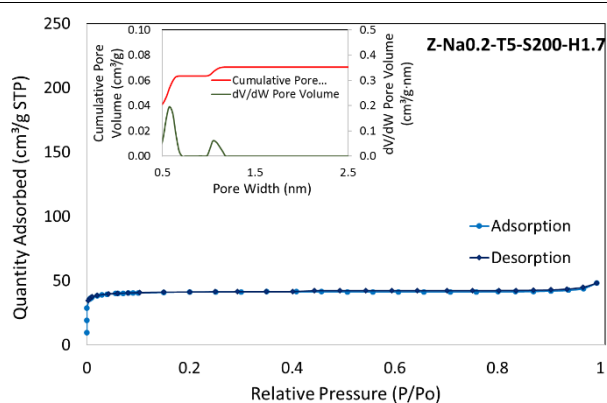
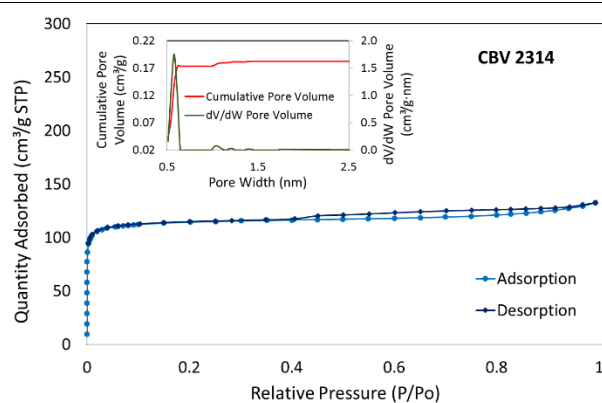
Appendix

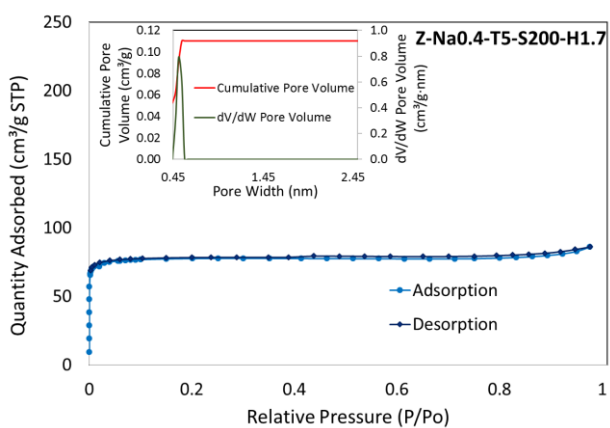
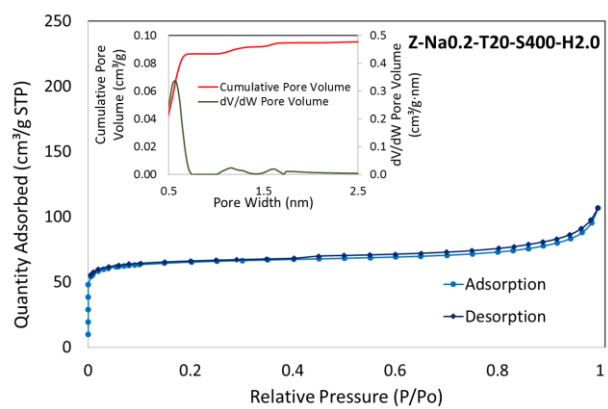
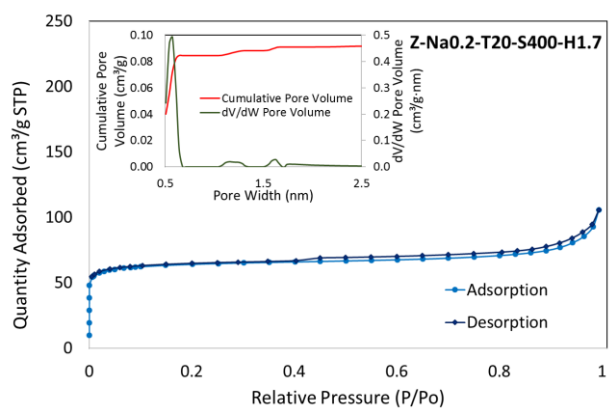
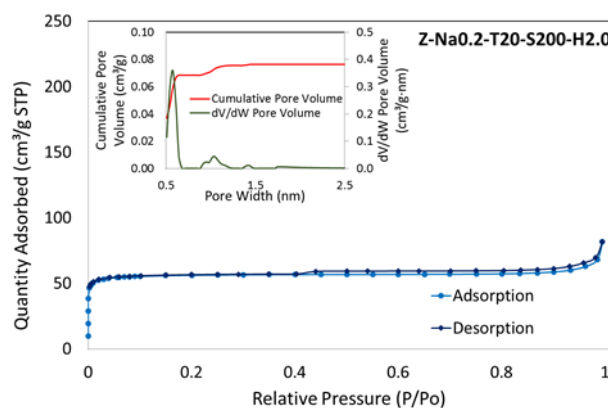
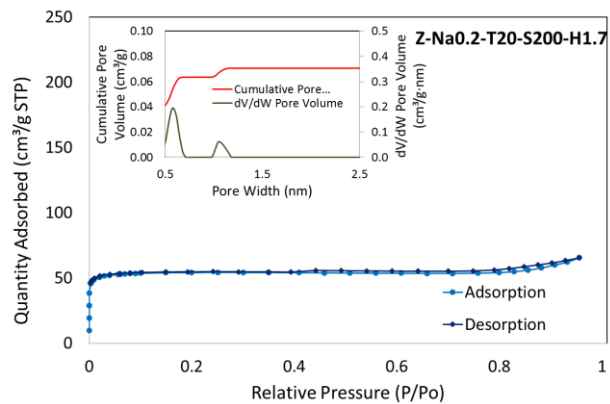
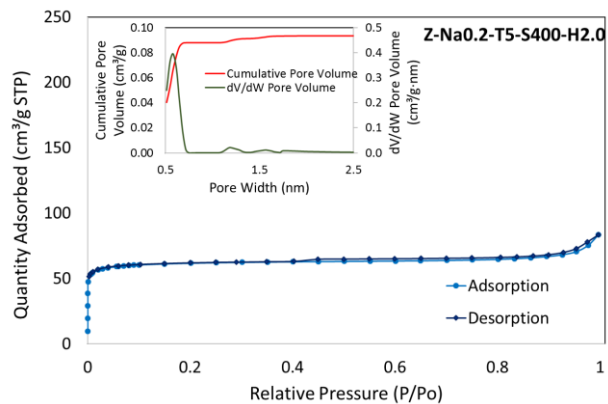
Appendix A

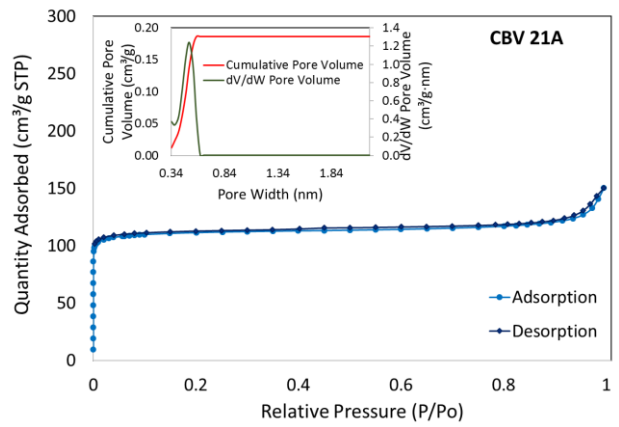
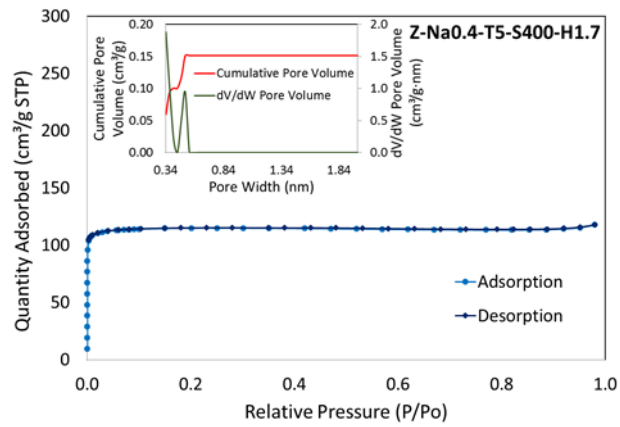
Table A1.

Ar (87 K) adsorption-desorption isotherms and pore size distribution of the synthesized samples.

The microporous range is determined using a pore adsorption NLDFT cylindrical model.







Appendix B

B.1. Surface area

Table B1 shows the ANOVA table that allows us to determine the synthesis variables that have a significant effect on the surface area. The effects were determined under the sparsity of effects principle, which allows studying an unreplicated factorial design (Montgomery, 1997). Variables and interactions that could affect are evidenced in the normal probability plot found in figure B1. In this method, the effects versus normal probability are plotted and data is adjusted to a straight line. Those data that deviate from said performane are evaluated in the ANOVA model, which was adjusted using the t-student test, due to the low amount of data. An $\alpha=0.05$ was used, with which it was determined that the only variable with a significant effect is the milling speed.

Table B1

ANOVA table of the synthesis variables effect on the surface area. B: Milling time, C: Milling speed and D: H_2O/SiO_2

Source	Sum of Squares	DF	Mean Square	F Value	P-Value
C	4255	1	4255	14.63	0.02
CD	277	1	277	0.95	0.38
BCD	20	1	20	0.07	0.81
Total	5696	7			
Residual	1164	4	291		

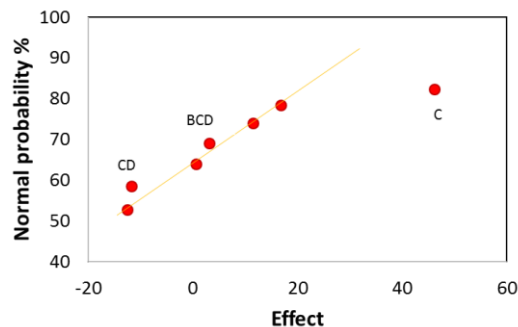


Figure B1. Normal probability of effects of the synthesis variables effect on the surface area. B: Milling time, C: Milling speed and D: $\text{H}_2\text{O}/\text{SiO}_2$

Figure B2 shows the double and triple effects plots. In this case, it is considered that there is a significant effect of the interaction of the synthesis variables if the lines intersect. It could be considered that the $C \times D$ interaction has an effect. However, when studying the DXC combination (its reciprocal), there is no intersection of the lines, so it is evident that there is no effect. In the ANOVA table, it was also found that although this combination could have an effect, it was not representative enough, coinciding with what was found in the effect graph.

In the case of the triple interaction, there is no crossing of lines in any of the combinations, which is consistent with the ANOVA table analysis.

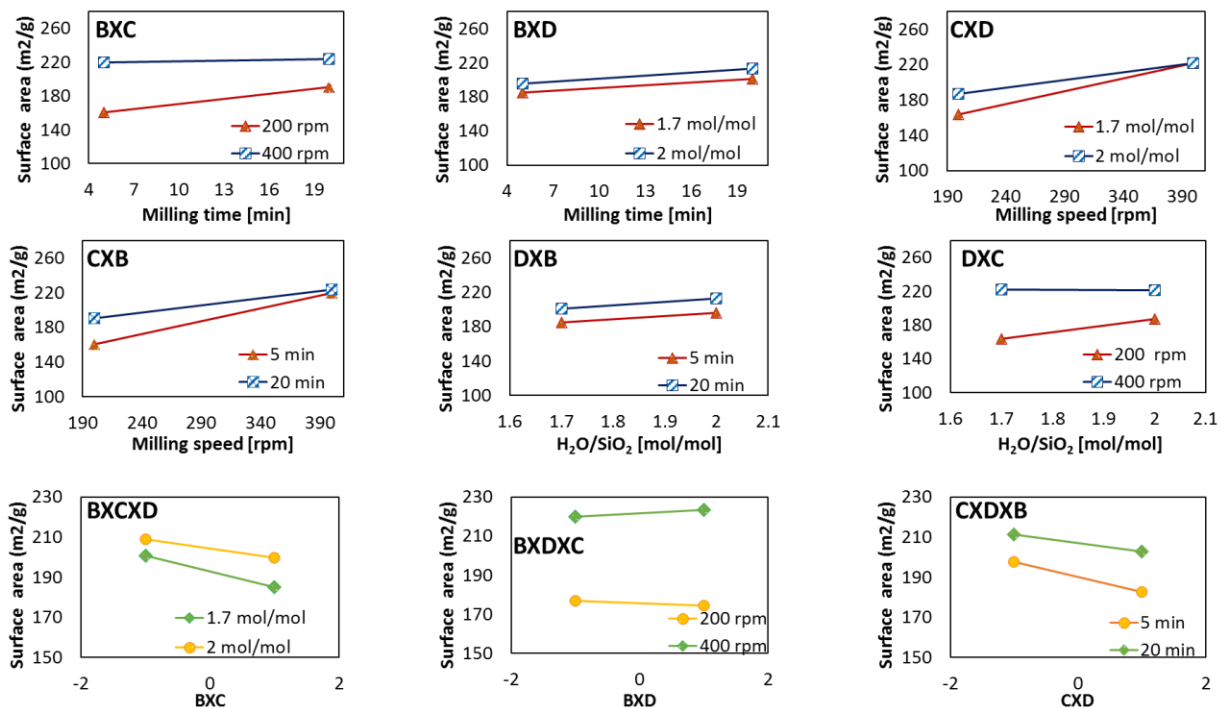


Figure B2. Graphs of double and triple effects of the synthesis variables on the surface area. B:

Milling time, C: Milling speed and D: H₂O/SiO₂

B.2. Crystallinity

Table B2 shows the ANOVA table for the crystallinity percentage, where it is observed that the only variable that has an effect is the milling speed.

Table B2

ANOVA table of the synthesis variables effect on the crystallinity percentage. B: Milling time, C: Milling speed and D: H₂O/SiO₂

Source	Sum of Squares	DF	Mean Square	F Value	P-Value
C	158.24	1	158.24	9.03	0.04
CD	0.41	1	0.41	0.02	0.89
BCD	0.02	1	0.02	0.00	0.98
Total	228.74	7			
Residual	70.09	4	17.52		

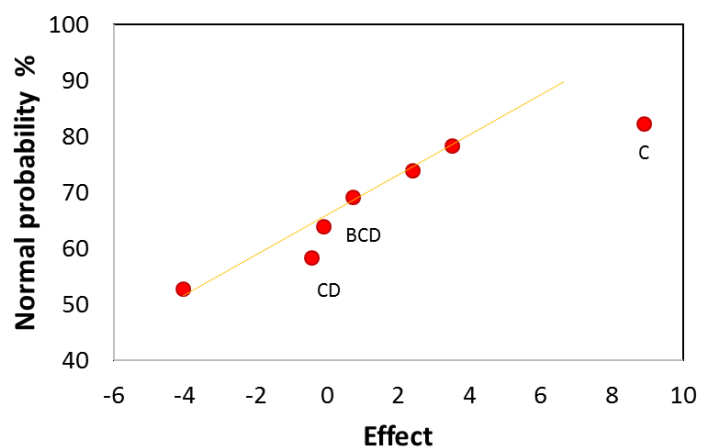


Figure B3. Normal probability of effects of the synthesis variables effect over crystallinity percentage. B: Milling time, C: Milling speed and D: H₂O/SiO₂

Figure B4 shows the double and triple interaction effects. In them, it is found that although it seems that the C_xB and D_xB interaction affect, the crossings show the opposite. Similarly, there is no triple interaction effect.

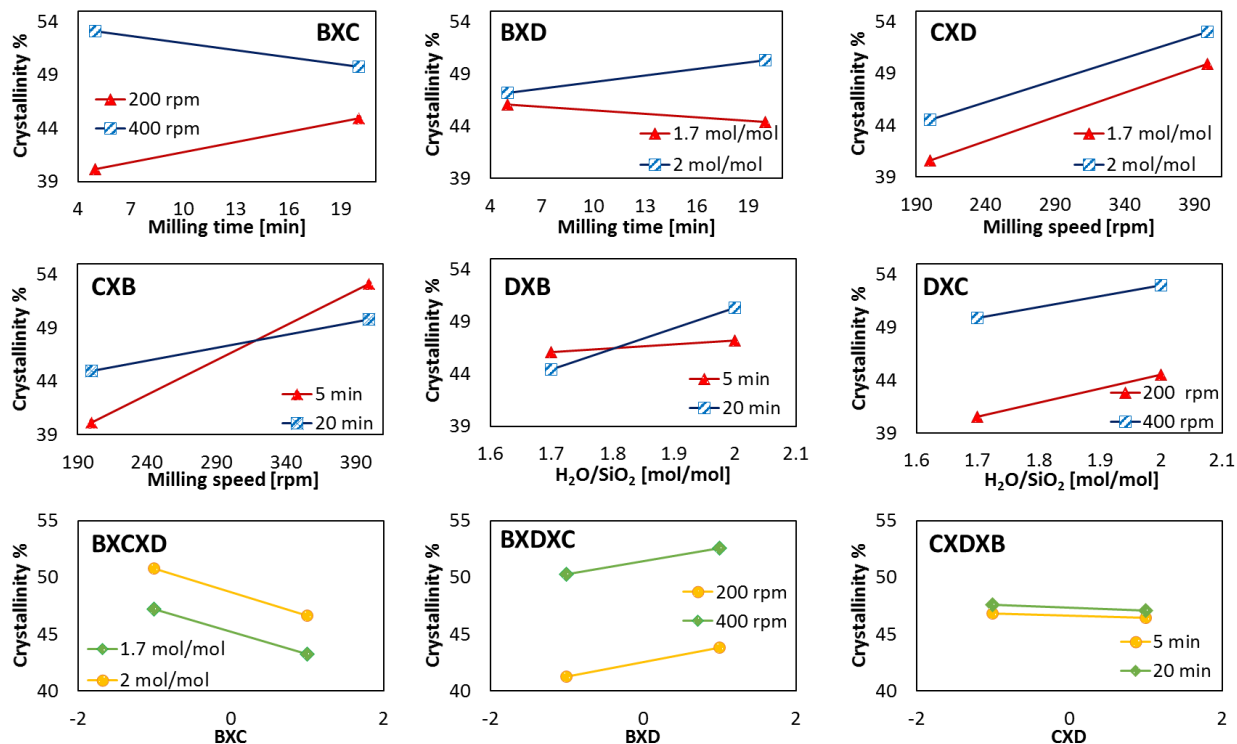


Figure B4. Graphs of double and triple effects of the synthesis variables on the crystallinity percentage. B: Milling time, C: Milling speed and D: H₂O/SiO₂

B.3. Phenol conversion

Table B3 contains the ANOVA table for the conversion of phenol. In this case, a 2³ factorial design with one replica was used. Therefore, normal probability plots were not used, and the effect of all variables and their interactions could be directly evaluated. The only variable that has a significant effect is the milling speed, which was evidenced in the main effects graphs of figure 16. Similarly, no effect of the double or triple combinations was found in the ANOVA table, not in the effect plots of figure B5.

Table B3

ANOVA table of the synthesis variables effect on the phenol conversion in the alkylation reaction. B: Milling time, C: Milling speed and D: H_2O/SiO_2

Source	Sum of Squares	DF	Mean Square	F Value	P-Value
B	1.6	1.0	1.6	2.6	0.15
C	22.7	1.0	22.7	36.9	0.00
D	1.2	1.0	1.2	1.9	0.20
BC	0.0	1.0	0.0	0.0	0.83
BD	1.9	1.0	1.9	3.1	0.12
CD	0.6	1.0	0.6	1.0	0.35
BCD	0.5	1.0	0.5	0.8	0.39
Total	33.4	15.0			
Residual	4.92	8	0.6		

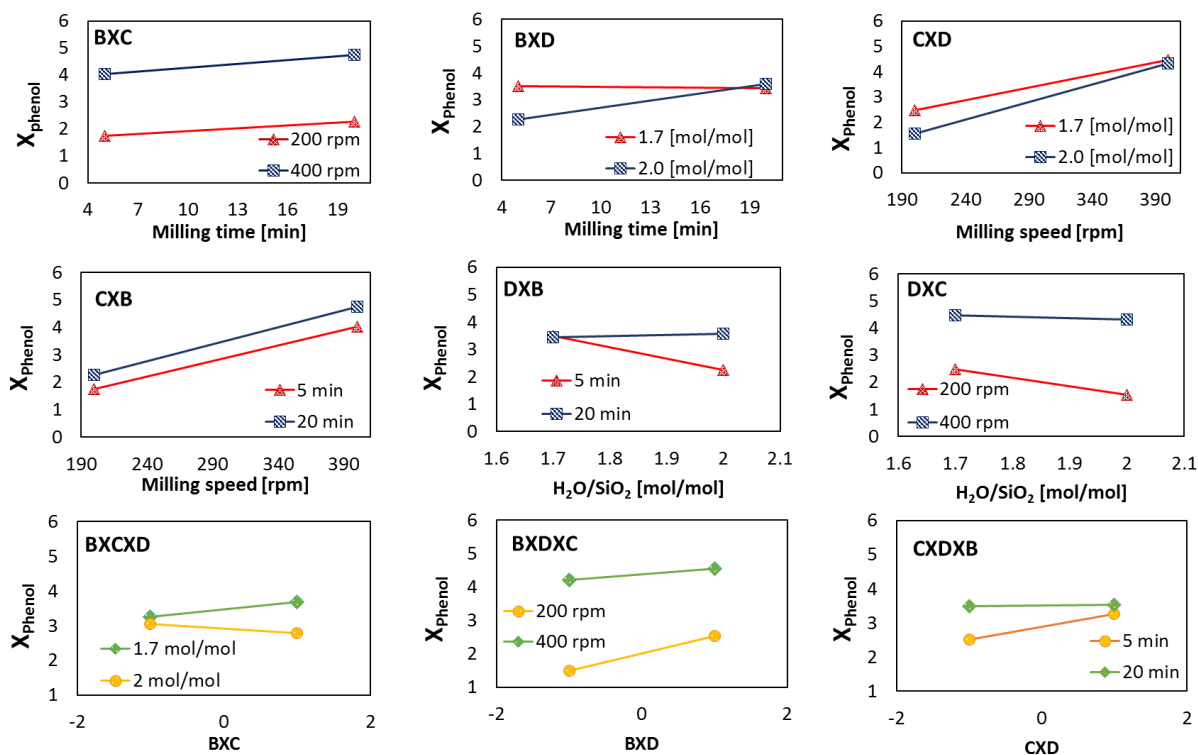


Figure B5. Graphs of double and triple effects of the synthesis variables on the phenol conversion in the alkylation reaction. B: Milling time, C: Milling speed and D: H_2O/SiO_2

B.4. Total acid sites

Table B4 contains the ANOVA table of the total acid sites number. None of the variables has a significant effect, which was evidenced in the main effect's graphs of figure 15. However, the milling speed has a significant effect. Besides, an effect of the double or triple combinations was not found in figure B7.

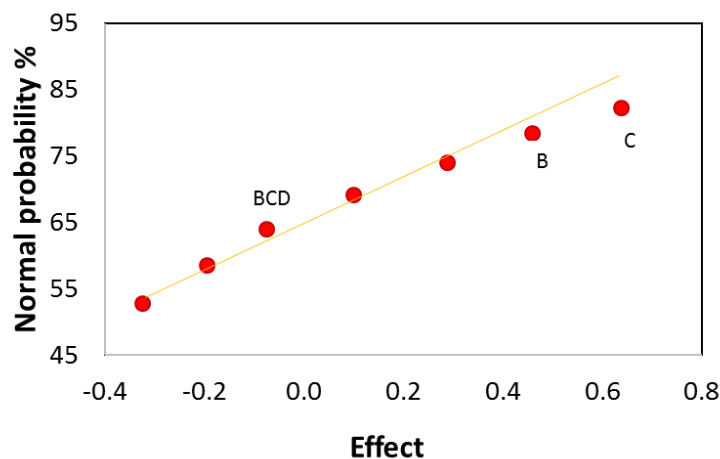


Figure B6. Normal probability of effects of the synthesis variables effect on the total acid sites B:

Milling time, C: Milling speed and D: H_2O/SiO_2

Table B4

ANOVA table of the synthesis variables effect on the total acid

sites. B: Milling time, C: Milling speed and D: H_2O/SiO_2

Source	Sum of Squares	DF	Mean Square	F Value	P-Value
B	0.42	1	0.42	3.47	0.14
C	0.81	1	0.81	6.69	0.06
BCD	0.01	1	0.01	0.09	0.77
Total	1.72	7			
Residual	0.49	4	0.12		

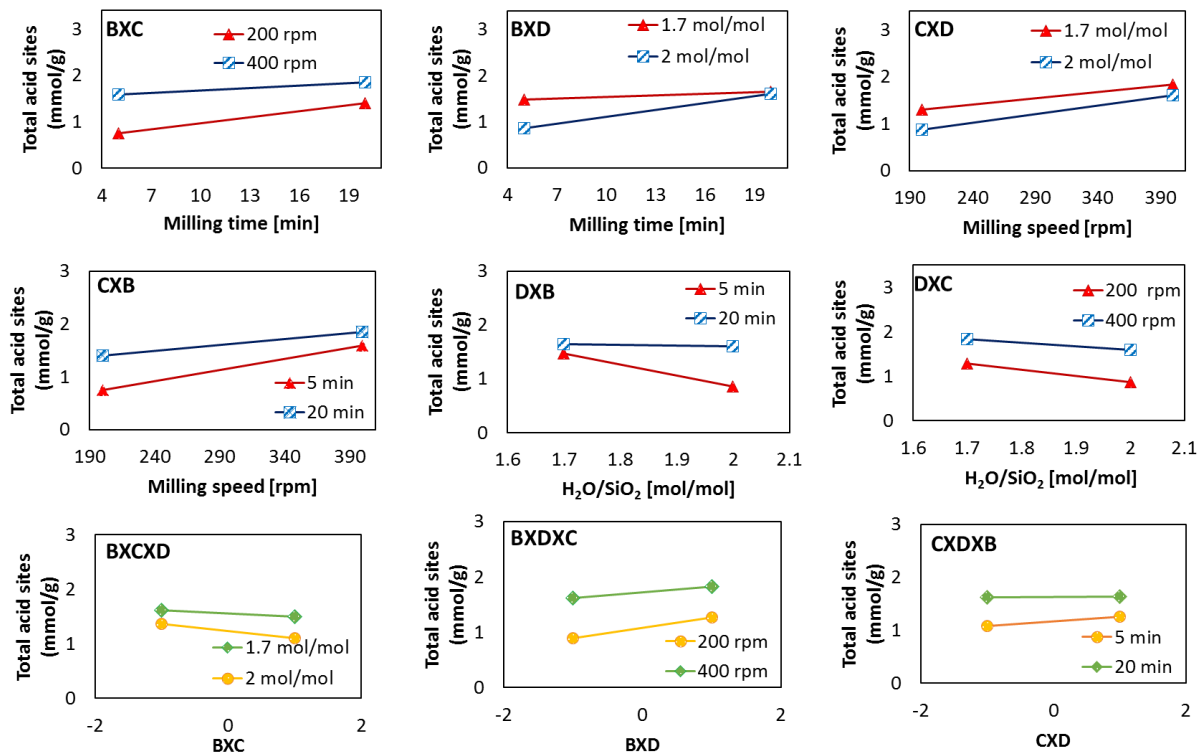


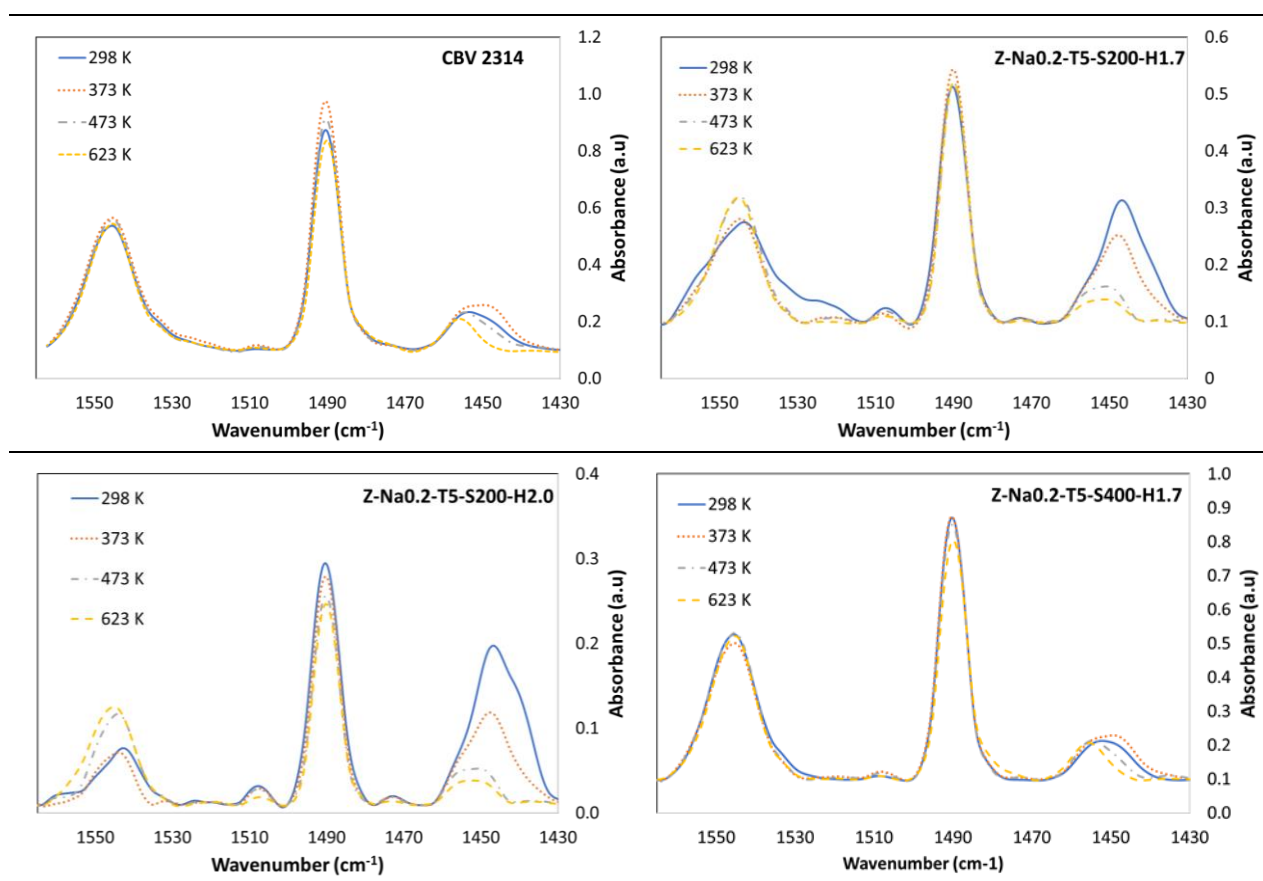
Figure B7. Graphs of double and triple effects of the synthesis variables on the total acid sites. B: Milling time, C: Milling speed and D: H₂O/SiO₂

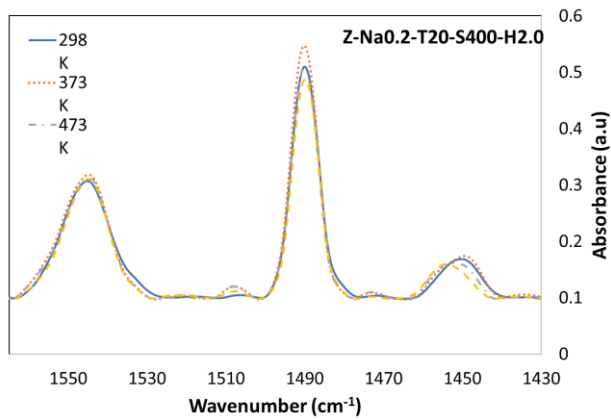
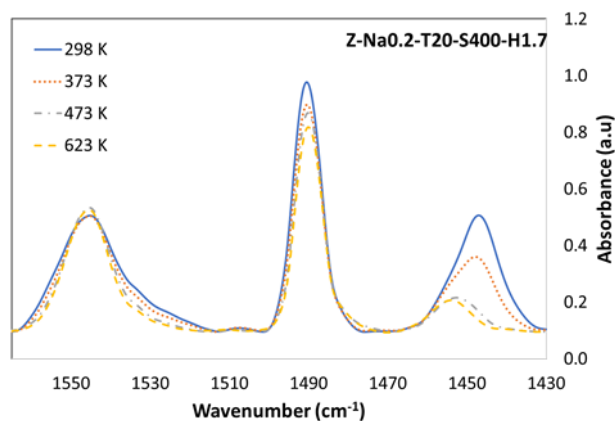
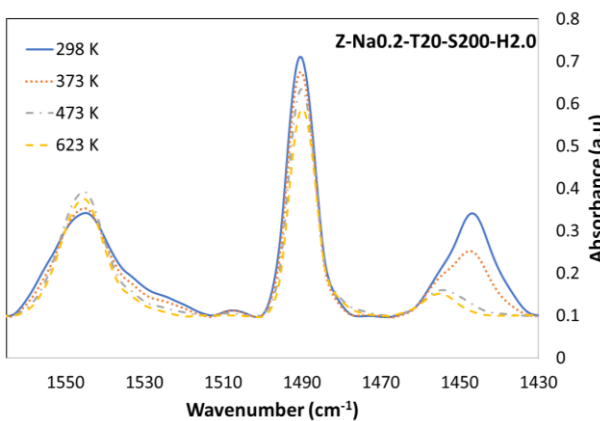
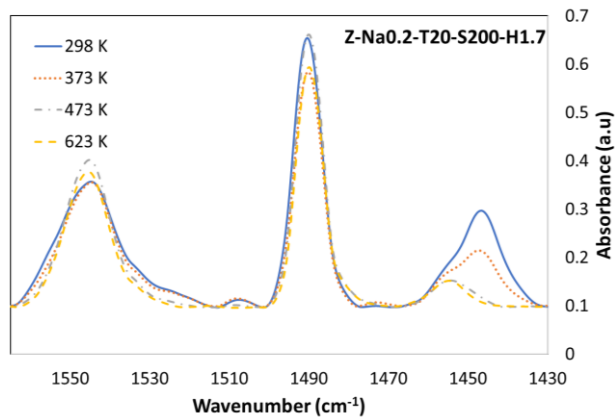
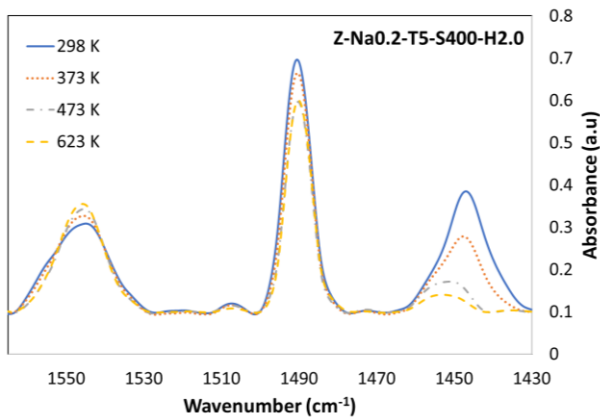
Appendix C

Table C1

FTIR spectra for pyridine TPD recorded of the synthesized zeolites at 298, 373, 473 and 623 K.

The highlighted bands correspond to pyridine adsorption on Brønsted (1545 cm^{-1}) and Lewis sites (1455 cm^{-1}). Band at 1491 cm^{-1} corresponds to an overlap of the signals from pyridine adsorbed on both the Brønsted and the Lewis sites and the band found at 1445 cm^{-1} corresponds to the physically adsorbed pyridine (Buzzoni, Bordiga, Ricchiardi, Lamberti, & Zecchina, 1996).





Appendix D

Table D1

Phenol and TBA conversion in the alkylation of phenol with tert-butyl alcohol using the synthesized samples and the seed as catalyst.

Sample	X_{Phenol}		X_{TBA}	
CBV 2314	3.9	3.7	39.8	40.0
Z-Na0.2-T5-S200-H1.7	2.8	2.2	19.3	27.1
Z-Na0.2-T5-S200-H2.0	0.7	0.8	16.5	20.4
Z-Na0.2-T5-S400-H1.7	4.5	4.1	40.2	38.9
Z-Na0.2-T5-S400-H2.0	3.8	2.8	38.8	39.9
Z-Na0.2-T20-S200-H1.7	2.3	2.9	39.9	32.9
Z-Na0.2-T20-S200-H2.0	2.2	2.4	30.8	27.5
Z-Na0.2-T20-S400-H1.7	4.5	4.8	39.2	51.9
Z-Na0.2-T20-S400-H2.0	4.9	4.0	40.9	40.2

Table D2

Selectivity of the alkylation of phenol with tert-butyl alcohol using the synthesized samples and the seed as catalyst.

Sample	2-TBP		4-TBP		3-TBP		2,4-DTBP		t-BPE	
CBV 2314	5.5	5.8	4.7	5.1	0.4	0.4	0.1	0.1	89.4	88.6
Z-Na0.2-T5-S200-H1.7	2.6	2.9	3.0	4.2	0.1	0.2	0.1	0.1	94.3	92.7
Z-Na0.2-T5-S200-H2.0	1.9	2.5	2.1	2.0	0.1	0.1	0.0	0.0	95.8	95.3
Z-Na0.2-T5-S400-H1.7	3.0	4.5	3.4	4.5	0.2	0.3	0.0	0.0	93.3	90.6
Z-Na0.2-T5-S400-H2.0	7.2	4.2	5.9	4.4	0.5	0.3	0.1	0.0	86.3	91.1
Z-Na0.2-T20-S200-H1.7	4.7	3.8	4.8	4.5	0.3	0.3	0.0	0.0	90.1	91.5
Z-Na0.2-T20-S200-H2.0	2.8	2.6	2.5	2.1	0.1	0.2	0.0	0.0	94.6	95.2
Z-Na0.2-T20-S400-H1.7	16.1	19.1	13.4	13.7	1.1	1.1	0.4	0.4	69.0	65.6
Z-Na0.2-T20-S400-H2.0	7.9	5.6	8.3	7.4	0.6	0.5	0.1	0.1	83.0	86.5
Z-Na0.4-T5-S200-H1.7	3.3		1.7		0.1		0.0		94.9	
Zp-Na0.2-T20-S400-H1.7	16.1	15.5	13.4	12.8	1.1	1.1	0.4	0.3	69.0	70.3
Z-Na0.2-T20-S500-H1.7	4.2		2.6		0.2		0.0		93.0	